CHEMISTRY OF MATERIALS
Review

Chem. Mater. **2010,** *22,* 6483–6505 6483
DOI:10.1021/cm101967h

ε-Fe_2O_3: An Advanced Nanomaterial Exhibiting Giant Coercive Field, Millimeter-Wave Ferromagnetic Resonance, and Magnetoelectric Coupling

Jiří Tuček,[†] Radek Zbořil,*[,†] Asuka Namai,[‡] and Shin-ichi Ohkoshi*[,‡]

[†]*Regional Centre of Advanced Technologies and Materials, Departments of Physical Chemistry and Experimental Physics, Faculty of Science, Palacky University, Slechtitelu 11, 783 71 Olomouc, Czech Republic, and* [‡]*Department of Chemistry, School of Science, The University of Tokyo, 7-3-1 Hongo, Bunkyo-ku, Tokyo 113-0033, Japan*

Received July 15, 2010. Revised Manuscript Received September 22, 2010

Nanosized iron oxides still attract significant attention within the scientific community, because of their application-promising properties. Among them, ε-Fe_2O_3 constitutes a remarkable phase, taking pride in a giant coercive field at room temperature, significant ferromagnetic resonance, and coupled magnetoelectric features that are not observed in any other simple metal oxide phase. In this work, we review basic structural and magnetic characteristics of this extraordinary nanomaterial with an emphasis on questionable and unresolved issues raised during its intense research in the past years. We show how a combination of various experimental techniques brings essential and valuable information, with regard to understanding the physicochemical properties of the ε-polymorph of Fe_2O_3, which remained unexplored for a long period of time. In addition, we recapitulate a series of synthetic routes that lead to the formation of ε-Fe_2O_3, highlighting their advantages and drawbacks. We also demonstrate how magnetic properties of ε-Fe_2O_3 can be tuned through the exploitation of various morphologies of ε-Fe_2O_3 nanosystems, the alignment of ε-Fe_2O_3 nanoobjects in a supporting matrix, and various degrees of cation substitution. Based on the current knowledge of the scientific community working in the field of ε-Fe_2O_3, we finally arrive at two main future challenges: (i) the search for optimal synthetic conditions to prepare single-phase ε-Fe_2O_3 with a high yield, desired size, morphology, and stability; and (ii) the search for a correct description of the magnetic behavior of ε-Fe_2O_3 at temperatures below the characteristic magnetic ordering temperature.

1. Introduction and Milestones in the Study of the ε-Fe_2O_3 Phase

Nanosized iron oxides still attract significant attention within the scientific community, because of their application-promising properties.[1−3] Besides technologically based application branches (e.g., magnetic recording media, information storage, magnetizable printing of copy, permanent magnets),[4,5] some of iron oxide phases have found their prospective utilizations in various fields of medicine[6−13] (e.g., drug delivery, medical diagnostics, ferrofluids) empowered by their magnetic properties (e.g., superparamagnetism, high values of saturation magnetization) and eminent biochemical characteristics (e.g., nontoxicity, biodegradability, biocompatibility). They are also important for theoretical studies (e.g., quantum tunneling of magnetization, effects of interparticle magnetic interactions on a magnetic regime of a nanoparticle system) when they are used as model systems to clear up certain magnetic features typical of nanoscaled objects, not observed in their bulk counterparts.[14]

Iron oxides represent the most common iron compounds found in nature, and, apart from some exceptions, they can be very easily synthesized. Until now, apart from amorphous iron(III) oxide, we have recognized six crystalline nonhydrated iron oxides:[4,15] Fe_3O_4 (i.e., magnetite); four polymorphs of Fe_2O_3, labeled as α-Fe_2O_3 (i.e., hematite), β-Fe_2O_3, γ-Fe_2O_3 (i.e., maghemite), and ε-Fe_2O_3; and FeO phase (i.e., wüstite). α-Fe_2O_3, γ-Fe_2O_3, and Fe_3O_4 are the most frequent iron oxides that exist in both bulk and nanosized forms and commonly occur in nature; in addition, there are a rich variety of synthetic routes to prepare them having thus many different morphologies, various sizes, and particle size distributions. In contrast, β-Fe_2O_3 and ε-Fe_2O_3, which were first observed in the laboratory, are regarded as rare phases with scarce natural abundance; they exist only as nanosized objects, it is very difficult to prepare them as single phases, and they are thermally unstable. Recently, renewed interest in the ε-polymorph of Fe_2O_3 has been encouraged by the discovery of its giant coercive field that is exhibited at room temperature and the coupling of its magnetic and dielectric properties.[16,17]

ε-Fe_2O_3 is a dark brown magnetic phase of iron(III) oxide. The natural occurrence of ε-Fe_2O_3 phase has been recently reported in some plants[18] (i.e., as biogenic

*Authors to whom correspondence should be addressed. Tel.: +420585634947 (R.Z.), +81-3-5841-4331 (S.O.). Fax: +420585634958 (R.Z.), +81-3-3812-1896 (S.O.). E-mail: zboril@prfnw.upol.cz (R.Z.), ohkoshi@chem.s.u-tokyo.ac.jp (S.O.).

Published on Web 10/27/2010

nanoparticles) and it has been found as a thermal decomposition product of almandine garnets[19] and iron-rich clays.[20,21] From the viewpoint of thermal phase transformations and crystal structures, it is considered as an intermediate phase that occurs, under certain circumstances, during the thermal conversion from a cubic spinel γ-Fe_2O_3 nanoscaled phase to a rhombohedral corundum α-Fe_2O_3 nanosized polymorph.[22−26] The crystal structure of ε-Fe_2O_3 phase is described as an orthorhombic noncentrosymmetric structure with Fe atoms occupying four distinct nonequivalent crystallographic sites, including one tetrahedral site and three different octahedral sites.[24,27−29] It exhibits a magnetic transition from a paramagnetic state to an ordered magnetic regime at a Curie temperature (T_C) of ~490 K.[24,30−32] However, its room-temperature ground magnetic state has been not unambiguously clarified. It is claimed that, at room temperature, it behaves either as a collinear ferrimagnet[16,24,29,33,34] or as a canted antiferromagnet.[28,35] In addition, at ~110 K, the ε-Fe_2O_3 phase undergoes another magnetic transition, accompanied by a series of structural transformations and spin reorientation phenomenon and manifested by a dramatic decrease in ε-Fe_2O_3 coercivity.[28,29,36,37] Again, two possible scenarios have been proposed. The results of various works show that the ε-polymorph of Fe_2O_3 magnetically transforms either from a ferrimagnetic state to some incommensurate magnetic structure (probably of a square-wave-modulated origin)[29,36] or from one canted antiferromagnetic state to another canted antiferromagnetic state with a possible metamagnetic behavior at low temperatures.[28,35]

This new crystalline polymorph of Fe_2O_3 was discovered by Forestier and Guiot-Guillain[38] in 1934, but it started to be labeled as ε-Fe_2O_3 by Schrader and Buttner[30] later in 1963. There had not been much attention devoted to this polymorph of iron(III) oxide until 1998, when Tronc et al.[24] reported the first detailed structural characterization of this phase, which was later refined independently by Sakurai et al.[37] and Kelm and Mader.[27] In 2004, Jin et al.[16] first synthesized a pure ε-Fe_2O_3 phase and observed a giant coercive field (B_C) of ~2 T exhibited by this rare iron(III) oxide polymorph at room temperature, which is widely regarded as one of the fundamental milestones in the research of the ε-Fe_2O_3 phase. Since the discovery of such a huge coercivity of ε-Fe_2O_3, which is quite unexpected for simple and single-valent iron oxides, many research works have emerged with the objective of preparing ε-Fe_2O_3 as a single phase,[16,27,28,39−49] to explain such a room-temperature magnetic hardness of ε-Fe_2O_3 and its drastic collapse observed at ~110 K,[16,36,37,50] to determine a correct magnetic phase diagram of ε-Fe_2O_3 as a function of temperature derived from various experimental data,[16,24,28,29,33−35] and even to enhance the value of the coercive field of ε-Fe_2O_3 somehow at room temperature.[51] However, the ε-polymorph of Fe_2O_3 is not easy to fabricate in the form of bare nanosized objects, because of its significant thermal instability. Thus, it turns out that either a certain degree of agglomeration in the precursor powders[26] and/or a need for a supporting medium[16,39,52] (e.g., silica matrix in most cases) play an essential role to synthesize the ε-Fe_2O_3 phase in the form of nanoparticles, nanorods, and nanowires. By that time, the last milestone concerning this remarkable nanomaterial is being connected with the work of Gich et al.,[53] who have first prepared ε-Fe_2O_3 as a thin film, thus enriching the family of already-existing ε-Fe_2O_3 nanoobjects.

Before the discovery and development of hard magnetic materials such as highly anisotropic magnetoplumbite barium hexaferrite ($BaFe_{12}O_{19}$), $SmCo_5$, $Nd_2Fe_{14}B$-type compounds, and FePt nanoparticles,[54,55] γ-Fe_2O_3 and/or Fe_3O_4 particles, modified later by an adsorption of suitable elements (e.g., cobalt), have been widely used in technological applications, including magnetic recording and information storage media.[4,56] Their utilization in the traditional magnetic recording media has been encouraged because of many advantages, such as availability, low cost, low toxicity, stability, high corrosion resistance, and high resistivity accompanied with low eddy-current losses.[57] However, since high-density magnetic recording requires very small nanoparticles still retaining significant magnetic hardness and uniform magnetization within the nanoparticle, γ-Fe_2O_3 and/or Fe_3O_4 phases become inapplicable by reason of a superparamagnetic phenomenon, connected with finite-size effects and manifested by a thermally activated spontaneous reversal of nanoparticle magnetization, and surface effects, reflected by inhomogeneous magnetization spatial profile within the surface layers of the nanoparticle, which they commonly exhibit at such demanded sizes of their nanoparticles at room temperature.[14,58−62] In addition, it, nevertheless, is not feasible to enlarge their coercive fields and make them thus magnetically harder, because of their low magnetocrystalline anisotropy constant controlled by their face-centered cubic crystal structure. This is not the case for the ε-Fe_2O_3 phase, which has a giant coercive field that is believed to be caused by a large magnetocrystalline anisotropy ($K_{MC} \approx (2-5) \times 10^5$ J/m^3) driven by an orthorhombic crystal structure, a low saturation magnetization ($M_S \approx 15-25$ Am^2/kg), the establishment of a single magnetic domain character due to conveniently sized nanoparticles, and a nonzero orbital component of the Fe^{3+} magnetic moment.[16,50] The value of the coercive field of the ε-Fe_2O_3 phase is much larger than that observed for hexagonal magnetoplumbite $BaFe_{12}O_{19}$ ($B_C \approx 0.64$ T) and/or hexagonally closed-packed cobalt and related Co-ferrites ($B_C \approx 0.74$ T) falling in the family of materials widely used in magnetic recording applications. Moreover, the coercivity of ε-Fe_2O_3 phase can be further increased by an alignment of its nanosized crystals (e.g., in the form of nanorods and/or nanowires) along a particular direction by an external magnetic field applied during the synthesis.[51] However, because of the relatively low saturation magnetization (and, thus, remanent magnetization) of the ε-Fe_2O_3 phase, which is reflected by weak magnetic forces to attract small metallic objects, it is not regarded as a good permanent magnet for hard magnetic utilizations, where a high residual magnetization of a material is required, along with its high coercivity. Nevertheless, because of its high coercivity, the ε-polymorph of Fe_2O_3 may become a promising candidate for a recording medium,

thanks to the high sensitivity of current giant-magnetoresistance-based reading devices. In addition, there is a growing interest in magnetic materials with a large coercivity expected to exhibit a high-frequency resonance with electromagnetic waves of millimeter wavelengths for effective suppression of the electromagnetic interference and stabilization of the electromagnetic transmittance.[63−65] Since the effect of high-frequency resonance has been recently reported in the ε-Fe_2O_3 phase and its Ga-substituted and Al-substituted analogs,[65,66] it unlocks the doors to possible applications of this Fe_2O_3 polymorph in electronic devices intended for high-speed wireless communication. In addition, because it possesses both spontaneous magnetization and polarization, it is being classified as an advanced magnetoelectric material with a possible applicability in various technological branches including electric/magnetic field-tunable devices.[17]

If synthesized as a pure phase and with a high yield, ε-Fe_2O_3 phase will definitely enter a class of the most important functional magnetic materials and its practical exploitation will probably enable the current material limits of certain technological applications, requiring materials with a considerable magnetic hardness, to be overcome and/or will give rise to new technological areas benefiting from its remarkable coupled magnetoelectric properties and ferromagnetic resonance capability, both unusual for simple iron oxides.

In this work, with regard to the significant application potential of the ε-Fe_2O_3 phase and an unresolved dispute that currently exists concerning the questions of its ground magnetic state and magnetic behavior at low temperatures, we briefly review its structural and magnetic characteristics, which have been either determined unambiguously or proposed so far. In this context, we also report on various synthetic routes, leading to nanosized ε-Fe_2O_3 with various morphologies, and point out the difficulties associated with its synthesis, phase purity, admixture problems, and phase stability. We also emphasize the effect of cation substitution, which seems to be an effective way of tuning the magnetic properties and subsequent possible applications of the ε-Fe_2O_3 phase. Taking into account various already published results of several research works, exploiting experimental techniques such as X-ray and neutron powder diffraction, zero-field and in-field temperature-dependent Mössbauer spectroscopy, and magnetization measurements, we finally discuss a physical picture of ε-Fe_2O_3 phase unwinding from its current knowledge put forward by the scientific community and considering an ambiguity in the description of its magnetism that still persists as an open issue.

2. Synthetic Routes toward the ε-Fe_2O_3 Phase

As has been already mentioned, the natural abundance of the ε-Fe_2O_3 phase is very limited. In addition, the ε-polymorph of Fe_2O_3 cannot be obtained in bulk form and exists only as a nanoparticle, because of its low surface energy,[52] thus suggesting an important role of the surface effects on its formation and existence. Being highly thermodynamically unstable, it very easily transforms to α-Fe_2O_3, which is considered to be the most thermodynamically stable phase out of all four crystalline polymorphs of Fe_2O_3.[15] It is very difficult to synthesize ε-Fe_2O_3 as a single product, because most of the synthetic routes lead to a mixture of ε-Fe_2O_3 with α-Fe_2O_3 and/or γ-Fe_2O_3 in varying contents, depending on the precursor used, utilization of the supporting matrix, the presence of Group IIA metal ions (e.g., Sr^{2+}, Ba^{2+}), and conditions secured during the synthesis.[16,22−28,30−32,39,40,67−71] For an analysis of physicochemical properties of ε-Fe_2O_3 and its subsequent promising applications, α-Fe_2O_3 and γ-Fe_2O_3 constitute an impurity and may drastically affect the overall physical behavior of the system, possibly leading to some incorrect conclusions. Note that, although some of the former works concerning the synthesis and study of ε-Fe_2O_3 reported a single-phase material,[30−32,38] subsequent renewals of the studies showed that yields of $> 70\%$ ε-Fe_2O_3 in the mixture are difficult to achieve.[15] Since most of the proposed syntheses are based on the growth of precursor nanoparticles toward the ε-Fe_2O_3 phase, a new strategy employing a supporting matrix with pores of definite sizes has been introduced to obtain much higher yields of ε-Fe_2O_3, either as a single phase[16] (without experimentally detected traces of admixtures of other iron oxide phases) or with an experimentally detectable but, in some cases, negligible portion of other Fe_2O_3 polymorphs.[22−24,39] Because of its highly porous structure that has restricted nanospaces with a high specific area,[72,73] mesoporous amorphous silica has been recently suggested to be a suitable medium for the controlled preparation of nanosized crystals of ε-Fe_2O_3. In other words, the porous nature of the amorphous silica matrix provides nucleating sites for ε-Fe_2O_3 nanoparticles and significantly prevents their aggregation, isolating the nanoparticles from each other. In addition, the confinement of ε-Fe_2O_3 nanoparticles within the pores of the supporting matrix enhances their thermal stability (see section 3). Generally, all the current synthetic routes that have been proposed for the preparation of ε-Fe_2O_3 imply that the formation of the ε-Fe_2O_3 phase is very sensitive to the synthesis conditions, such as oxidizing power of the atmosphere, duration of the oxidation, and/or the presence of hydroxyl groups (i.e., excess water, high hydrolysis ratio, etc.).[39]

So far, two different morphologies of ε-Fe_2O_3 nanoparticles have been reported in the literature, i.e., sphere (or spherelike) shapes[22−24,26,28,29,36,39,46−49,67−71] and nanorod (nanowire) shapes.[16,27,40,42−45,51] Recently, ε-Fe_2O_3 has been synthesized as a thin film $\sim$100 nm thick.[53] In the case of spherical ε-Fe_2O_3 nanoparticles, their diameter ranges from $\sim$10 nm to > 200 nm,[39,41] whereas nanorods (nanowires) are typically $\sim$20 nm to 2 μm long and $\sim$10−50 nm wide (see Figure 1).[40,43,45] The systems that are comprised of either ε-Fe_2O_3 nanospheres or ε-Fe_2O_3 nanorods (nanowires) generally exhibit a size distribution character that is presumably governed by the particular synthesis method and its conditions and/or, in some cases, by the particle size distribution of the precursor (e.g., in methods based on thermal transformations of Fe_2O_3 polymorphs and Fe_3O_4). The sphere morphologies of ε-Fe_2O_3 can be obtained via the thermal

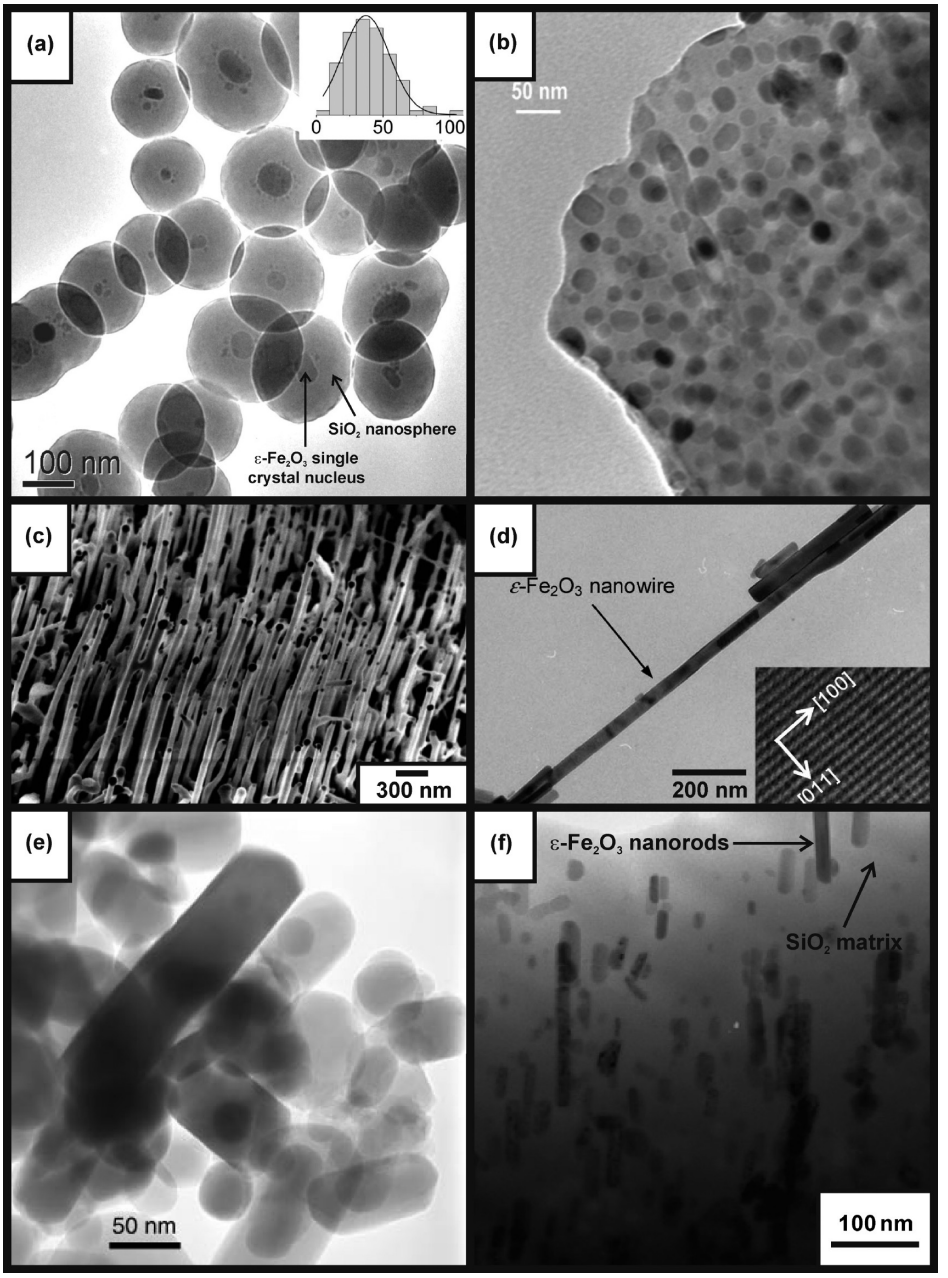

Figure 1. Representative examples of various morphologies of the ε-Fe_2O_3 phase: nanospheres and nanoparticles (top row), nanowires (middle row), and nanorods (bottom row). Panel (a) has been taken from Taboada et al.,[49] panel (b) has been taken from Popovici et al.,[39] panel (c) has been taken from Morber et al.,[42] panel (d) has been taken from Sakurai et al.,[45] panel (e) has been taken from Kelm and Mader,[27] and panel (f) has been taken from Sakurai et al.[51]

decompositions of suitable iron-containing precursors[26,38] or their oxidation advanced by high-energy deposition techniques, including electric discharge,[30] gamma irradiation,[74] laser-assisted pyrolysis,[75] and sol−gel methods, followed by heat treatments at a certain temperature and for a definite time.[28,39,46,76] On the other hand, nanorods and nanowires of ε-Fe_2O_3 can be synthesized employing combination of the reverse-micelle and sol−gel methods (where $Fe(NO_3)_3$ is used as a precursor),[45] microemulsion/sol−gel method (where $Fe(NO_3)_3$ is used as a precursor),[16,40,51] and/or by vapor−liquid−solid mechanisms assisted by pulsed laser deposition (where Fe_3O_4 is used as a precursor).[42,43] Preparation techniques based on thermal decompositions and oxidation involve heat treatment of Fe-bearing precursors such as a mixture of Fe_2O_3 polymorphs, Fe_3O_4, basic ferric salts, and other precipitates derived from the ferric iron salts in basic solutions. Concerning high-energy deposition synthetic methods, they promote the oxidation of vaporized iron, iron(II) formate, and an $Fe(CO)_5$−N_2O gas mixture. In the case of sol−gel methods, often iron nitrate[22−24,77] (i.e., $Fe(NO_3)_3$) and/or yttrium iron garnet (i.e., $Y_3Fe_5O_{12}$)[28,35,67−71,78] are mixed with silicon alkoxides (e.g., tetraethoxysilane (TEOS) and $Si(C_2H_5O)_4$) and, upon heating to a certain temperature, nanocomposites of ε-Fe_2O_3/SiO_2 are formed. In general, the sol−gel method is comprised of four steps: (i) hydrolysis, (ii) condensation, (iii) drying, and (iv) thermal treatment. Recently, a new sol−gel approach for the preparation of ε-Fe_2O_3/SiO_2 nanocomposites has been reported when a single precursor (i.e., ethylenediaminetetraacetic acid dianhydride (EDTA)) involving both functional groups for

silica matrix and iron oxide has been used.[48] However, some authors have noted the disadvantages of a sol−gel method connected with the existence of silica impurities and small grain size of synthesized ε-Fe_2O_3 nanoparticles, which normally falls below 200 nm.[43] To get an overview of the possible reaction routes toward ε-Fe_2O_3, several synthesis methods, including some historical works, are presented below.

As previously stated, the first synthesis of the ε-Fe_2O_3 phase was reported by Forestier and Guiot-Guillain, who carried out a thermal decomposition of $Fe_2O_3 \cdot 4BeO$ and found a formation of Fe_2O_3 phase unknown by that time.[38] Almost 30 years later, this new Fe_2O_3 polymorph, along with α-Fe_2O_3 and γ-Fe_2O_3, was obtained by Schrader and Buttner,[30] using a method based on the electric arc discharge of an iron oxide aerosol under an oxidizing atmosphere. They were the first authors who called it ε-Fe_2O_3. Subsequently, Walter-Lévy and Quemeneur prepared a mixture of ε-Fe_2O_3 with α-Fe_2O_3 by heating a basic sulfate salt (i.e., calcination of $6Fe_2(SO_4)_3 \cdot Fe_2O_3 \cdot nH_2O$).[79] This suggests that the mixing of Fe atoms and OH groups in a nanoparticle seems to be crucial to prepare ε-Fe_2O_3 nanocrystals. The ε-Fe_2O_3 phase can be also synthesized upon boiling an aqueous mixture of potassium ferricyanide ($K_3[Fe(CN)_6]$), sodium hypochlorite (NaClO), and potassium hydroxide (KOH), as it was shown by Trautmann and Forestier[31] and later by Dezsi and Coey.[32] However, similar to the case of the previously mentioned preparation routes, this synthetic procedure does not yield a single ε-Fe_2O_3 phase since α-Fe_2O_3 and possibly γ-Fe_2O_3 polymorphs are also produced in a certain amount. Thus, to eliminate the appearance of phase impurities associated with the synthesis of ε-Fe_2O_3, there was a necessity to develop a completely different synthetic approach. As previously stated, the usage of a supporting matrix (organic polymers or inorganic silica matrix in most cases) has opened up a new strategy to synthesize ε-Fe_2O_3 nanoparticles with a higher yield and a significantly lower portion of undesired other Fe_2O_3 polymorphs. It was encouraged by Nižňanský et al.,[80] who reported that the thermal stability of metastable iron oxides can be readily increased by encapsulation of the nanoparticles into a silica matrix. The spatial restriction of nanoparticle growth definitely represents a crucial point for the production of ε-Fe_2O_3 nanoparticles, as reported by Chanéac et al.[22] and Zboril et al.,[26] who prepared ε-Fe_2O_3 with α-Fe_2O_3 with and without a supporting matrix, respectively. Their results show that, at a certain temperature range, the restricted agglomeration of γ-Fe_2O_3 nanoparticles favors the formation of the ε-Fe_2O_3 phase, which converts to the α-Fe_2O_3 polymorph upon subsequent heating. With a silica matrix enhancing the thermal stability of precursor γ-Fe_2O_3 nanoparticles, the γ-$Fe_2O_3 \rightarrow \varepsilon$-$Fe_2O_3$ transformation is observed to occur at temperatures higher than 1300 K.[39] In the case of an absence of the supporting matrix but meeting the requirement of the limited agglomeration of precursor γ-Fe_2O_3 nanoparticles, this phase transformation occurs at much lower temperatures (>700 K)[26] and the as-formed ε-Fe_2O_3 nanoparticles are readily prone to the conversion to α-Fe_2O_3 nanoparticles upon subsequent thermal treatment. However, if a large number of γ-Fe_2O_3 nanoparticles are sintered, we straightly get an α-Fe_2O_3 phase, as in the case of powdered γ-Fe_2O_3 nanoparticles, where the phase transformation to α-Fe_2O_3 is observed from ~600 K to ~1300 K.[81] An interesting formation of ε-Fe_2O_3 nanoparticles has been described by Taketomi et al.[67] In their synthetic procedure, amorphous yttrium−iron garnet nanoparticles were dispersed in a kerosene solvent and these colloids were then introduced into the nanosized pores of controlled porous glass. After a high-temperature treatment, a very small fraction of the uncalcined amorphous nanoparticles has been consequently spontaneously crystallized to ε-Fe_2O_3 nanocrystals. Recently, Barick et al.[82] focused on the synthesis parameters that affect the preparation of ε-Fe_2O_3 nanoparticles, employing the sol−gel method with an inorganic SiO_2 matrix. They have found that changing the synthesis conditions, such as the concentration of precursor Fe^{3+} ions and the temperature of thermal treatment, leads to a random or homogeneous dispersion of ε-Fe_2O_3 nanoparticles with a different size distribution and with a different degree of γ-Fe_2O_3 admixture. In addition, it has been confirmed that the chemical environment of Fe^{3+} ions and the gel structure undergo several changes, depending on the concentration of precursor Fe^{3+} ions and the temperature of thermal treatment.

A remarkable synthesis of ε-Fe_2O_3 has been proposed by Kelm and Mader.[27] They obtained an ε-Fe_2O_3 powder material via thermal decomposition of the clay mineral nontronite ($(CaO_{0.5},Na)_{0.3}Fe_2(Si,Al)_4O_{10}(OH)_2 \cdot nH_2O$) at 900−970 °C and subsequent isolation of the ferric oxide by leaching the silicate phases. In addition, they showed that crystals of ε-Fe_2O_3 can grow as precipitates via the internal oxidation of a $Pd_{96}Fe_4$ alloy. Kusano et al.[44] have recently emphasized that no supporting matrix is needed to produce pure ε-Fe_2O_3 phase. They observed ε-Fe_2O_3 nanoparticles crystallizing epitaxially on needlelike crystals of mullite (i.e., $3(Al,Fe)_2O_3 \cdot 2SiO_2$), formed after heat treatment of Japanese traditional stoneware known as "Bizen" clay (composed of quartz (SiO_2), halloysite ($Al_2O_3 \cdot 2SiO_2 \cdot 4H_2O$), montmorillonite ($(Na,Ca)_{0.33}(Al,Mg)_2(Si_4O_{10})(OH)_2 \cdot nH_2O$), and feldspar ($(Na,K)AlSi_3O_8$) as the main crystalline phases) covered by a rice straw. Interestingly, it was found that the crystal shape and size of ε-Fe_2O_3 nanoparticles and their relative orientations, with regard to needlelike mullite crystals, remarkably change with oxygen partial pressure.

Most of the synthetic routes mentioned above involve a temperature-induced phase transformation from γ-Fe_2O_3 to ε-Fe_2O_3 in their final step. Thus, the well-known γ-$Fe_2O_3 \rightarrow \varepsilon$-$Fe_2O_3 \rightarrow \alpha$-$Fe_2O_3$ pathway is widely recognized as an easy way to prepare ε-Fe_2O_3 nanoparticles, where γ-Fe_2O_3 acts as a precursor phase. However, some works indicate other iron oxides to be a source material for the formation of ε-Fe_2O_3. Ding et al.[43] have recently reported the synthesis of ε-Fe_2O_3 nanowires upon thermal conversion of Fe_3O_4 (i.e., the $Fe_3O_4 \rightarrow \varepsilon$-$Fe_2O_3$ pathway), which is believed to happen because of either an overabundance of iron and/or an oxygen deficiency in the starting phase.

In addition, the authors claim that, if oxygen had absorbed into the lattice (or iron desorbed from the lattice) in a random manner, leaving Fe site occupation nonperiodical, γ-Fe_2O_3 would preferentially form.[43] Thus, the formation of ε-Fe_2O_3 is understood as a result of a perfectly ordered species evolution. It is shown that if Fe_3O_4 nanowires grow along the Fe_3O_4 [110] direction, the ε-Fe_2O_3 phase is found in every instance, fulfilling a fixed structural relationship of $(001)_{\varepsilon\text{-}Fe_2O_3} \parallel (111)_{Fe_3O_4}$, $[010]_{\varepsilon\text{-}Fe_2O_3} \parallel \langle 110\rangle_{Fe_3O_4}$. Since the nanowires grown along this crystallographic direction reach the longest lengths, compared to those grown along other investigated directions (i.e., [111] and $\langle 211\rangle$ directions), Ding et al.[43] supposed that the nanowires growing along the fast-growth Fe_3O_4 [110] nanowire direction allow an Fe_3O_4-to-ε-Fe_2O_3 oxidation to occur, because of their surfaces being sufficiently exposed to an oxidative process. In contrast to the well-known phase transformation route between various Fe_2O_3 polymorphs, Tadic et al.[47] observed the formation of an ε-Fe_2O_3 phase upon the heat treatment of 4 nm α-Fe_2O_3 nanoparticles dispersed in a silica matrix. However, according to our opinion and experience, this route seems to be highly improbable, taking into account the considerably higher thermal stability of the α-Fe_2O_3 polymorph, compared to the ε-Fe_2O_3 phase.

According to the results of the phase transformation studies, it is expected that the ε-Fe_2O_3 phase converts to the α-Fe_2O_3 polymorph if the particle size (i.e., a diameter in the approximation of spherelike nanoobjects) exceeds a value of ~30 nm. Larger ε-Fe_2O_3 nanoparticles, with sizes up to 100−200 nm, can be prepared and are stable when an appropriate amount of Group IIA metal ions (e.g., Sr^{2+} or Ba^{2+} ions) are added into the reaction system.[16,40,41] It was proposed that the presence of Group IIA metal ions causes an acceleration of growth of ε-Fe_2O_3 nanoparticles and enhances their thermal stability against the transformation to the α-Fe_2O_3 polymorph. In other words, the alkaline-earth ions control the growth and size of resulting Fe_2O_3 nanoparticles in the silica matrix. In addition, because the Ba^{2+} ions have been shown to adsorb preferably onto the crystal planes of (010) or (001) being parallel to the *a*-axis of ε-Fe_2O_3 crystal, it allows one to synthesize ε-Fe_2O_3 nanowire structures that grow along the respective axis.[45] It also appears that the amount of Ba^{2+} ions also has an impact of the phase purity of the synthesized nanoparticle system. If the Fe/Ba ratio ranges from 10 to 20, a single ε-Fe_2O_3 phase is formed. However, if more Ba^{2+} ions are added, it results in prevailing formation of the α-Fe_2O_3 polymorph.[40] To date, this synthetic approach employing Group IIA metal ions and a silica matrix definitely represents the way to produce the purest ε-Fe_2O_3 phase without any other iron(III) oxide polymorphs (especially α-Fe_2O_3 and/or γ-Fe_2O_3) as admixtures, since they have not been detected by various experimental techniques, allowing the analysis of the sample phase composition, including recently employed zero-field and in-field Mössbauer spectroscopy.

Recently, the ε-Fe_2O_3 phase has been first synthesized as an epitaxial thin film ~100 nm thick with (001) texture via pulsed laser deposition.[53] These thin films were grown on several substrates, including Si(100), MgO(110), yttria-stabilized zirconia(111), and STO(111). The authors claim that the alternating Ti^{4+} and SrO_3^{4-} layers, having 3-fold symmetry in the STO(111) substrate, serve as nucleation sites for ε-Fe_2O_3 basal planes. However, because of the large crystal lattice mismatch between the STO substrate and the ε-Fe_2O_3 film, it is believed that only very small domains (of a few nanometers) have been nucleated, showing atomically sharp interfaces. The authors speculate that the stabilization of the ε-Fe_2O_3 phase is governed by this domain structure, rather than by an epitaxial strain, because the observed domain structure causes minimization of the energy of ε-Fe_2O_3(100) surfaces.

3. Crystal and Magnetic Structure of the ε-Fe_2O_3 Phase, Phase Transformations, and Substitutions by Foreign Cations

From the crystallographic viewpoint, ε-Fe_2O_3 exhibits an orthorhombic crystal structure with a space group of $Pna2_1$ and lattice parameters $a = 5.072$ Å, $b = 8.736$ Å, $c = 9.418$ Å, and $\alpha = \beta = \gamma = 90°$.[27,37] The structure is isomorphous to that of $GaFeO_3$, $AlFeO_3$, and κ-Al_2O_3. Formerly, the crystal structure of ε-Fe_2O_3 has been reported as being deformed rhombohedral[38] or monoclinic,[30] but the Rietveld refinements of powder X-ray diffraction pattern (XRD) were very poor, in contrast to the later proposed orthorhombic crystal family,[24,83] which is currently being widely recognized as a correct description of ε-Fe_2O_3 crystal structure.[27,37] The orthorhombic unit cell of ε-Fe_2O_3 consists of triple chains of edge-sharing FeO_6 octahedra running along the *a*-axis, which are connected to each other by sharing corners of the FeO_6 octahedra, leaving one-dimensional cavities that are filled by the chains of the corner-sharing tetrahedra (see Figure 2). Thus, the crystal structure of ε-Fe_2O_3 contains four independent crystallographically nonequivalent iron sites, i.e., three different octahedral sites (denoted hereafter as the A-, B-, and C-sites) and one tetrahedral sites (denoted hereafter as the D-sites), and the structure is polar being similar to that of $MM'O_3$, where M = Al, Ga, or Fe and M′ = Fe. Based on the refined atomic coordinates by Rietveld analysis, it has been found that all four cation coordination polyhedra, i.e., three octahedra and one tetrahedron, exhibit a different degrees of distortion (see Figure 3).[29] Taking into account the measured values of the parameter (Δ) that describes the degree of distortion of the cation coordination polyhedron, it turns out that two of the octahedral iron sites are more distorted, compared to the distortion displayed by the third octahedral site. From this aspect, the A- and B-sites are said to possess distorted octahedral coordination, while the C-site is regarded as having a regular octahedral coordination. These distortions, especially those which occur in the local environment of the octahedral A- and B-site and the tetrahedral D-site, seems to be of crucial importance to understand the magnetic characteristics of ε-Fe_2O_3 phase, since they are responsible for a generation of a nonzero orbital component to the total Fe^{3+} magnetic moment, leading to an unexpectedly significant spin−orbit coupling phenomenon in this Fe_2O_3 polymorph (see below).[50] In addition, the magnetic frustration due to site topology

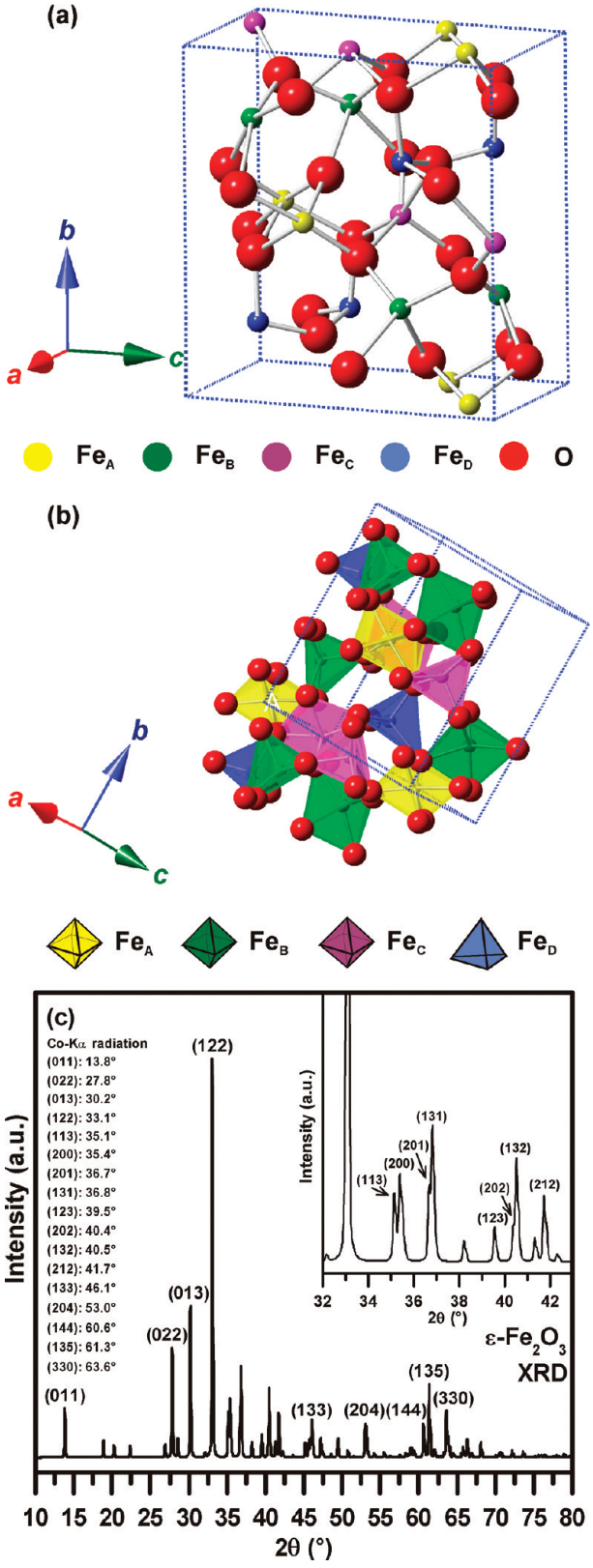

Figure 2. (a) Schematic representation of the unit cell of the ε-Fe_2O_3 phase employing ball-stick model, (b) crystallographic structure of the ε-Fe_2O_3 phase represented by the cation polyhedra, and (c) typical XRD pattern of the ε-Fe_2O_3 phase at room temperature, with the major atomic planes assigned to the corresponding Miller indices.

cannot be excluded a priori. To secure the valence consideration, all Fe atoms are trivalent and in the high spin state (i.e., $S = 5/2$) as a result of a weak ligand field. In contrast to

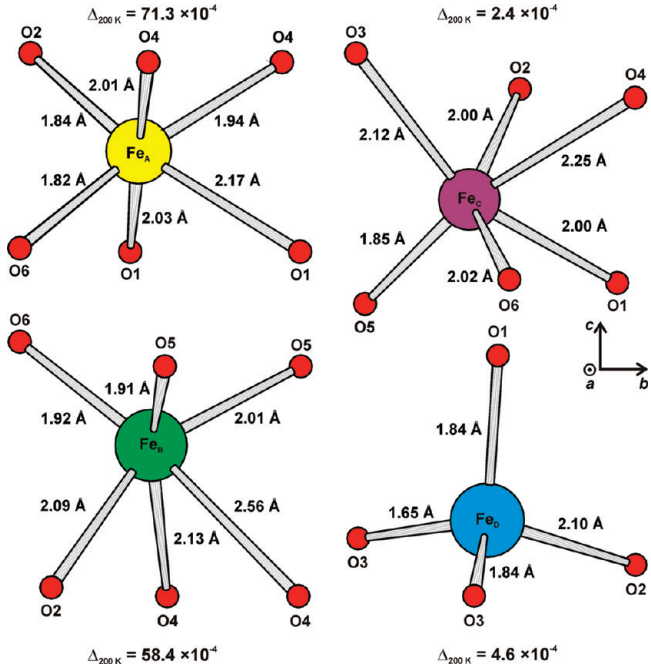

Figure 3. Details of various crystallographic Fe sites in the crystal structure of the ε-Fe_2O_3 phase showing the bond lengths at 300 K (plotted from XRD data presented by Kelm and Mader[27] and included in the Inorganic Crystal Structure Database (ICSD No. 415250)) and distortions, $\Delta_{200\,K}$, of cation polyhedra at 200 K (distortion values taken from Gich et al.[29] and calculated as $\Delta = (1/n)\sum_{i=1}^{n}[(D_i - D)/D]^2$, where D_i is the distance to a given neighbor, $\langle D \rangle$ the average distance to the first neighbor, and n the coordination number).

γ-Fe_2O_3, all cation crystallographic sites are occupied by Fe atoms with no vacant sites in the crystal structure. In fact, the crystal structure of ε-Fe_2O_3 involves similarities with both the structure of γ-Fe_2O_3 (a cubic spinel structure composed of a tetrahedron of four-coordinated Fe^{3+} ion and an octahedron of six-coordinated Fe^{3+} ion) and the structure of α-Fe_2O_3 (a rhombohedral structure consisting of stacked sheets of octahedrally coordinated Fe^{3+} ions between two closed-packed layers of oxygens).[15]

The existence of four nonequivalent Fe sites in the crystal structure of ε-Fe_2O_3 predestinates its magnetic structure. Therefore, ε-Fe_2O_3 is said to be a 4-sublattice magnetic material, characterized by four sublattice magnetizations with different temperature behaviors. The ordered magnetic regime of ε-Fe_2O_3 is driven by antiferromagnetic superexchange interactions that occur between Fe atoms intermediated by an O atom placed between them. To gain insight into the strength of individual superexchange interactions between Fe atoms belonging to different magnetic sublattices in the structure of ε-Fe_2O_3, there recently has been an attempt to calculate the values of the exchange integrals corresponding to various intersublattice exchange paths theoretically.[34] The model, employing the molecular field theory, defines individual sublattice magnetizations, denoted as M_A, M_B, M_C, and M_D, where M_A, M_B, and M_C are the sublattice magnetizations that are related to the three different octahedral sites, whereas M_D represents the sublattice magnetization on the tetrahedral sites. During the calculation, it is found that M_B and M_C are positive sublattice magnetizations, whereas M_A and M_D are negative

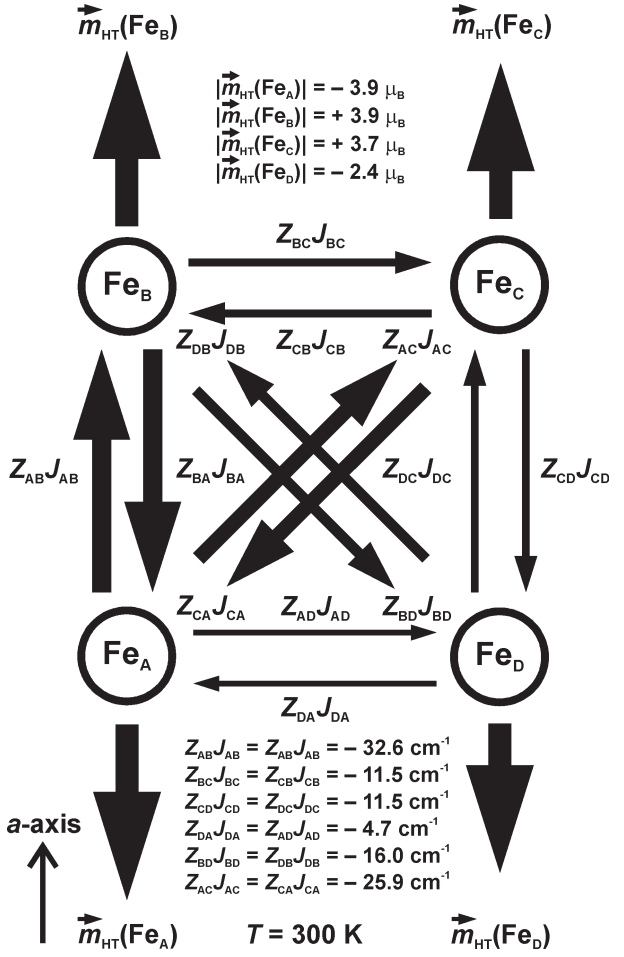

Figure 4. Schematic diagram describing the arrangement of magnetic moments of Fe atoms occupying various crystallographic sites in the structure of the ε-Fe_2O_3 phase including the magnitudes of iron magnetic moments and the values of $Z_{ij}J_{ij}$ parameters at 300 K. (Adapted from Ohkoshi et al.[34])

sublattice magnetizations. The $M_{total} = (M_B + M_C - M_A - M_D)$ value of ε-Fe_2O_3 then shows a maximum at 338 K and reaches zero at 0 K, which implies that ε-Fe_2O_3 is a Néel P-type ferrimagnet. Taking into account the number of exchange pathways (described by the Z_{ij} parameter, where i, j = A, B, C, D) that exist between respective Fe^{3+} ions via several oxygen ions, it was found that M_A and M_D, and M_B and M_C are parallel to each other, respectively, whereas M_A and M_D are antiparallel to both M_B and M_C (see Figure 4). The values of the effective exchange integrals (J_{ij}) were estimated to be $J_{AB} = -5.43\ cm^{-1}$, $J_{AC} = -4.32\ cm^{-1}$, $J_{AD} = -4.67\ cm^{-1}$, $J_{BD} = -3.99\ cm^{-1}$, and $J_{CD} = -3.85\ cm^{-1}$.[34] Since the sublattice magnetization of the tetrahedral magnetic sublattice is smaller in magnitude than the sublattice magnetizations for the octahedral sites, the model implies an imperfect antiferromagnetic ordering with an uncompensated overall magnetization of the structure that manifests itself as a ferromagnetic component. In other words, M_D determines the value of the net magnetization of ε-Fe_2O_3. This theoretically derived magnetic ordering of ε-Fe_2O_3 sublattice magnetizations is observed to correspond with the results of room-temperature neutron diffraction measurements performed by Gich et al.[29] Their neutron diffraction study introduces two different states of ordering of magnetic moments of Fe^{3+} ions in one tetrahedral and three different octahedral crystallographic sites, as a function of temperature. At higher temperatures (generally above 150 K and below 490 K, denoted hereafter by the abbreviation "HT"), the magnetic moments ($m_{HT}(Fe_i)$, i = A, B, C, and D) of Fe^{3+} ions point along the crystallographic a-axis with $m_{HT}(Fe_A) = -3.9\ \mu_B$, $m_{HT}(Fe_B) = 3.9\ \mu_B$, $m_{HT}(Fe_C) = 3.7\ \mu_B$, and $m_{HT}(Fe_D) = -2.4\ \mu_B$.[29] In other words, following Figure 4, Fe^{3+} magnetic moments occupying distorted octahedral A- and B-sites mutually cancel, because of their perfect antiparallel arrangement and the net magnetization of ε-Fe_2O_3 arises as a result from magnitude-uncompensated oppositely aligned Fe^{3+} magnetic moments sitting at the regular octahedral C-sites and tetrahedral D-sites. Based on these values of magnetic moments of Fe^{3+} ions at different crystallographic sites, it is then easy to show that we get a net magnetization of $\sim 0.3\ \mu_B$ per Fe^{3+} ion at 300 K, which is in accordance with the experimental value found from the magnetization measurements and in-field Mössbauer spectroscopy (see sections 4 and 5). Such a low net magnetization value offers two possible conclusions, concerning the room-temperature magnetic ground state of ε-Fe_2O_3. It behaves either as a collinear ferrimagnet[16,24,29,33,34] or as a canted antiferromagnet;[28,35] still, agreement regarding this issue has not been reached within the scientific community yet. However, at low temperatures (below 110 K), the HT arrangement of the magnetic moments of Fe^{3+} ions in the structure of ε-Fe_2O_3 does not match the experimental data from low-temperature neutron diffraction, which suggests a different magnetic ground state. At ~110 K, a disappearance of (011) and (120) magnetic reflections is observed, followed by a rise of new magnetic peaks near these two reflections. These new peaks are satellites of the (011) and (120) Bragg positions, implying an emergence of an incommensurate magnetic structure below ~110 K (see Figure 5).[29,36] After testing various helimagnetic and sine-modulated structures to fit the profiles of the low-temperature neutron diffraction patterns, it turned out that, below 110 K, the ordering of magnetic moments of tetrahedrally and octahedrally coordinated Fe atoms becomes rather complicated, which can be correctly described by a sine-modulated structure with a periodicity of ~10 crystalline unit cells and with all Fe^{3+} magnetic moments lying in the xy-plane. However, this does not appear to be an absolutely correct description of the low-temperature magnetic ordering of atomic magnetic moments within the four crystallographic sites, as noted by the Mössbauer spectroscopy results.[29] The spectral components of the Mössbauer spectra (four sextets ascribed to four different crystallographic sites), measured at 10 and 200 K, exhibit almost the same line width values for all of the sites, which suggests that the sextets related to the Fe^{3+} ions located at the particular crystallographic sites of ε-Fe_2O_3 structure are quite narrow and, consequently, the corresponding magnetic moments of Fe^{3+} ions should be almost constant in modulus. Indeed, this is not fulfilled in the case of a sine-modulated magnetic structure with a periodicity of ~10 unit cells. Thus, to satisfy the neutron diffraction data

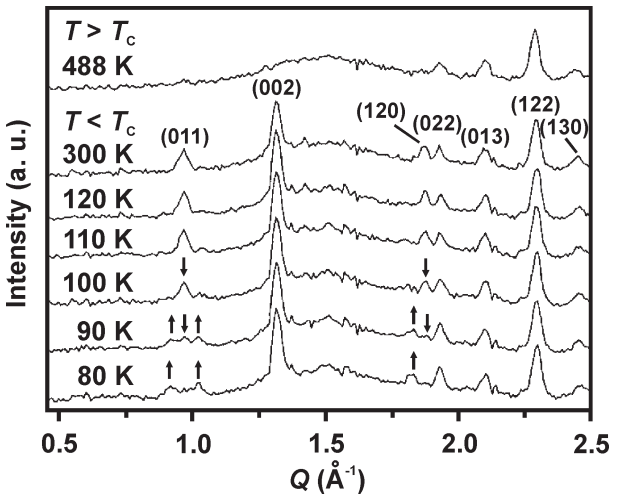

Figure 5. Neutron diffraction patterns of ε-Fe_2O_3 nanoparticles embedded in the silica matrix measured at 80, 90, 100, 110, 120, 300, and 488 K. The most relevant reflections are indicated for the pattern at 300 K, and the arrows mark the appearance and disappearance of relevant magnetic diffraction peaks as the temperature decreases. (Adapted from Gich et al.[36])

and the results derived from the Mössbauer spectra, a square-wave-modulated magnetic structure (i.e., the superposition of a series of sine-modulated structures with the harmonics of wave vectors as the propagation vectors) has been finally proposed to characterize the low-temperature magnetic state of Fe^{3+} magnetic moments in ε-Fe_2O_3. At this point, a crystallographic phase transformation cannot be excluded unambiguously, since most of the magnetic transitions occur simultaneously with the structural changes.

The conclusions stemming from the results of neutron diffraction measurements obtained by Gich et al.[29] have been recently confirmed by Tseng et al.[50] Similar to that reported in the work by Gich et al.,[29] it was proposed that the transition from high-temperature commensurate magnetic structure to low-temperature incommensurate magnetic structure occurs in at least three stages between 80 K and 150 K. In this temperature interval, changes in the coordination of octahedral A-sites and tetrahedral D-sites are assumed to occur that arise simultaneously and/or as a consequence of the emergence of the incommensurate magnetic regime. This second-order structural transition dampens out below 80 K and ε-Fe_2O_3 enters a magnetic state characteristic of a square-wave incommensurate magnetic structure. Occurring along with this gradual magnetic transition, Tseng et al.[50] observed a change in the strength of spin−orbit coupling caused by instability in the orbital contribution (m_{orb}) to the Fe^{3+} magnetic moment. It has been shown that, while the spin component (m_{spin}) of the Fe^{3+} magnetic moment remains temperature-independent, as the temperature falls down, the orbital component of the Fe^{3+} magnetic moment first reduces, reaching its minimum value at ~120 K, after which it strengthens back to attain a value of the same order as that at 200 K (see Figure 6). In other words, spin−orbit interactions weaken, leading to partial loosening of a tight bond between m_{spin} of the Fe^{3+} magnetic moment and strong local crystal electric fields generated

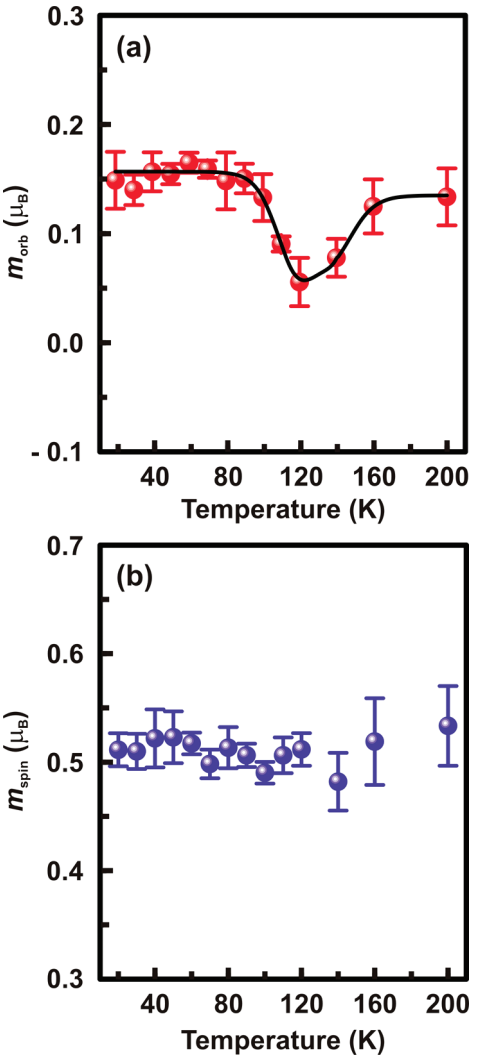

Figure 6. Temperature dependence of (a) the effective orbital moment (m_{orb}) and (b) effective spin moment (m_{spin}) of the Fe^{3+} magnetic moment in the ε-Fe_2O_3 phase. (Adapted from Tseng et al.[50])

by surrounding (oxygen) ions. This remarkable behavior of m_{orb} is closely connected with the lattice distortions and structural changes (the *c*-axis suffers an increased contraction, in contrast to the *a*- and *b*-axis, as documented by results from temperature-dependent XRD) that accompany the magnetic transition from a high-temperature commensurate to low-temperature incommensurate magnetic ordering in ε-Fe_2O_3. This is then manifested in the decrease of magnetocrystalline anisotropy constant and a drastic decline of coercivity at ~110 K. In addition, combining the analyses of experimental data from XRD, magnetization measurements, and Mössbauer spectroscopy indicates that significant changes in m_{orb} of Fe^{3+} ions and the collapse of coercivity in ε-Fe_2O_3 appear only in a limited temperature range (80−150 K). Because a change in the profile of the neutron diffraction pattern of ε-Fe_2O_3 has been also detected in this temperature interval,[28] all the experimental results thus unambiguously confirm the existence of the magnetic transition at ~110 K, driven by structural changes involving distortions predominately affecting the surroundings of the A- and D-sites.[29] However, similar to that observed

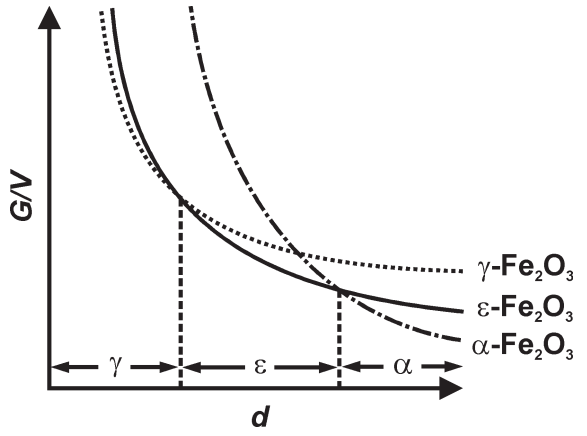

Figure 7. Stability of individual polymorphs of Fe_2O_3 based on the calculated dependence of the free energy per volume (i.e., G/V) on the size (d) of the iron(III) oxide nanoparticles of a particular polymorph (the dependences derived under the conditions of $\mu_\alpha < \mu_\varepsilon < \mu_\gamma$, $\sigma_\alpha > \sigma_\varepsilon > \sigma_\gamma$, and $(\sigma_\varepsilon - \sigma_\gamma)/(\mu_\varepsilon - \mu_\gamma) > (\sigma_\varepsilon - \sigma_\alpha)/(\mu_\varepsilon - \mu_\alpha)$). (Adapted from Ohkoshi et al.[40])

above 150 K, there are still doubts about the nature of the ground magnetic state of ε-Fe_2O_3 at low temperatures, since some authors claim that a transition at ~110 K separates two canted antiferromagnetic regimes with different canting angles rather than a collinear ferrimagnetic and square-wave incommensurate magnetic state (see section 5).[28,35]

As it has been already mentioned, this fourth polymorph of iron(III) oxide exists only in the form of nanoobjects. Since it is thermodynamically unstable, it easily transforms to α-Fe_2O_3 upon heating.[15] This phase transformation is accompanied by the size increase of the iron(III) oxide nanoparticles (i.e., the transformation is triggered at the temperature when the size of the ε-Fe_2O_3 nanoparticles reaches a certain value above which they become thermodynamically unstable). In unconfined samples (i.e., space-unrestricted ε-Fe_2O_3 nanoparticles), a wide range of temperatures (from ~700 K to ~1300 K) have been reported for the ε-$Fe_2O_3 \rightarrow \alpha$-$Fe_2O_3$ transformation.[38,75] However, if confined in the pores of a silica matrix with defined sizes, the stability of ε-Fe_2O_3 is enhanced, shifting the transformation temperature even to ~1700 K.[22] The presence of a silica matrix thus prevents the growth of ε-Fe_2O_3 nanoparticles within the silica pores, avoiding particle coalescence.

In general, there are two main factors that affect what Fe_2O_3 nanosized polymorph is formed from a precursor and how it is transformed to various iron(III) oxide phases.[40,53] These include the free energy (G) per volume (V) of different i-Fe_2O_3 phases ($i = \alpha, \beta, \gamma, \varepsilon$), and the energy barrier that must be overcome for the phase transformation to occur. These two parameters are dependent on many factors, including the kinetics and nanoscaled nature (e.g., enhanced surface-to-volume ratio) of a material. The free energy (or, equivalently, the Gibbs energy) per volume then takes into account the chemical potential (μ) and the surface energy (σ), i.e., $G/V = (\mu/\upsilon) + (6\sigma/d)$, where υ is the molar volume and d denotes the size of a nanoparticle. Generally, it is widely accepted that the surface energy and surface stress, being characteristic nanoparticle parameters, act as driving forces for the formation and stability of crystalline phases. Considering these facts, one can easily derive that the ε-Fe_2O_3 phase can exist when the size of the Fe_2O_3 particle is $-6\upsilon(\sigma_\varepsilon - \sigma_\gamma)/(\mu_\varepsilon - \mu_\gamma) < d < -6\upsilon(\sigma_\varepsilon - \sigma_\alpha)/(\mu_\varepsilon - \mu_\alpha)$ if (i) $\mu_\alpha < \mu_\varepsilon < \mu_\gamma$, (ii) $\sigma_\alpha > \sigma_\varepsilon > \sigma_\gamma$, and (iii) $(\sigma_\varepsilon - \sigma_\gamma)/(\mu_\varepsilon - \mu_\gamma) > (\sigma_\varepsilon - \sigma_\alpha)/(\mu_\varepsilon - \mu_\alpha)$ (see Figure 7).[40] Thus, it follows that, if Fe_2O_3 nanoparticles grow large enough, the existence of an ε-Fe_2O_3 phase is no longer favored. In other words, the size reduction of the Fe_2O_3 particle enhances a contribution of the surface (or interface) energy to the Gibbs free energy, which stabilizes the ε-Fe_2O_3 phase in the nanoscaled size. The validity of this rule has been recently supported by the work of Sakurai et al.,[84] who succeeded to first observe a successive phase transformation that included all four crystalline polymorphs of Fe_2O_3 (i.e., the γ-$Fe_2O_3 \rightarrow \varepsilon$-$Fe_2O_3 \rightarrow \beta$-$Fe_2O_3 \rightarrow \alpha$-$Fe_2O_3$ phase transformation) upon increasing the Fe_2O_3 particle size precisely. In the synthesis employing a silica matrix as a size restrictor and $FeSO_4$ as a precursor, the threshold sizes (diameters of spherical nanoparticles) at which the $\gamma \rightarrow \varepsilon$, $\varepsilon \rightarrow \beta$, and $\beta \rightarrow \alpha$ phase transformations occur were estimated to be ~8 nm, ~30 nm, and ~50 nm, respectively.

So far, few works have been focused on the effect of substitution of non-Fe cations in the structure of ε-Fe_2O_3. None of the works, published to date, has confirmed any dependence of the morphology of ε-Fe_2O_3 nanoobjects upon cation substitution; the morphology of the cation-substituted ε-Fe_2O_3 nanoobjects does not change with the replacement of Fe^{3+} ions by foreign metal cations.[65,66,85,86] On the other hand, the average particle size and particle size distribution have been found, to some extent, to be dependent on a degree of cation substitution; however, its effect does not follow any definite rule (i.e., it does not correlate with a substitution-induced evolution of other physical quantities whose dependences on the degree of cation substitution can be described by an explicit rule).[65,66,85,86] One of the first substitution-oriented studies involved gallium-doped ε-Fe_2O_3 rod-shaped nanoparticles (i.e., ε-$Ga_xFe_{2-x}O_3$, where $0.10 \le x \le 0.67$), because it turns out that these nanomagnets are promising for a construction of a millimeter-wave absorber exhibiting ferromagnetic resonance in the region of 35−147 GHz (see section 7).[65] It was shown that the substitution of Ga^{3+} ions occurs preferentially at the D-sites and partially at the octahedral C-sites, whereas the two distorted octahedral sites are not doped, as a result of a smaller ionic radius of Ga^{3+} (0.620 Å), compared with that of Fe^{3+} (0.645 Å). As the amount of Ga^{3+} ions increases in the structure of ε-Fe_2O_3, it leads to a progressive compression of the lattice constants. In addition, the amount of gallium substitution controls the value of the net magnetization, reaching a value of ~30 Am^2/kg for ε-$Ga_{0.47}Fe_{1.53}O_3$ at 300 K, which is almost twice as high as the room-temperature net magnetization value reported for undoped ε-Fe_2O_3 (see section 5). However, exceeding a certain amount of Ga atoms in the structure of ε-Fe_2O_3 (if $x > 0.47$ in ε-$Ga_xFe_{2-x}O_3$), the value of the room-temperature net magnetization decreases as Ga atoms begin to substitute for Fe atoms, preferentially at the C-sites.[85] Apart from this, the degree of Ga^{3+} substitution affects the value of the coercive field at 300 K,

which can be tuned over a wide range. As more Ga atoms are substituted in the structure of ε-Fe_2O_3, the value of the room-temperature coercivity decreases, which is believed to happen because of the progressive decrease in the Curie temperature with increasing Ga^{3+} substitution.[85] Similar substitution-driven effects on the structural and magnetic properties of the ε-Fe_2O_3 phase have been observed for aluminum-doped ε-Fe_2O_3 nanomagnets (i.e., ε-$Al_xFe_{2-x}O_3$, where $0.06 \leq x \leq 0.40$), which are being considered as another perspective candidate in the field of electromagnetic wave absorbers for high-speed wireless communication.[66] Within the substitution range studied, it has been found that the Al^{3+} ion prefers to occupy the D-sites, because of its smaller ionic radius (0.535 Å), compared to that of the Fe^{3+} ion. As the aluminum content increases in the crystal structure of ε-Fe_2O_3, the lattice parameters are progressively reduced, as in the case of Ga^{3+} substitution.[66] Upon an increase of doped Al^{3+} ions, the Curie temperature and room-temperature coercivity (B_C(300 K)) of aluminum-substituted ε-Fe_2O_3 nanosystems gradually decrease, whereas the room-temperature net magnetization (M(300 K/5 T)) in an applied magnetic field of 5 T increases, in comparison to the corresponding values of T_C, B_C(300 K), and M(300 K/5 T) reported for an undoped ε-Fe_2O_3 phase.[66] However, if In^{3+} ions are gradually substituted in the crystal structure of ε-iron(III) oxide polymorph (i.e., ε-$In_xFe_{2-x}O_3$, where $0.12 \leq x \leq 0.24$),[86] the lattice constants describing the crystal structure of undoped ε-Fe_2O_3 phase progressively enlarge as a result of the bigger ionic radius of the In^{3+} ion (0.790 Å) than that of the Fe^{3+} ion. In contrast to the site occupation preference observed for Ga^{3+} and Al^{3+} substituting ions, In^{3+} ions predominantly occupy the distorted octahedral A- and B-sites of ε-Fe_2O_3 crystal structure. Similar to that observed in the case of Ga^{3+} and Al^{3+} substitution, the values of T_C and B_C(300 K) decrease as the concentration of doped In^{3+} ions increases.[86] However, no change in the M(300 K/5 T) values has been observed within the investigated range of In^{3+} substitution.

4. Zero-Field and In-Field Mössbauer Spectroscopy of the ε-Fe_2O_3 Phase

As it is well-known, ^{57}Fe Mössbauer spectroscopy is a very sensitive experimental tool; it allows one to monitor the changes in the local environment of the Fe atoms in the crystal lattice. Hyperfine parameters, obtained from the spectral line positions, such as the isomer shift (δ), quadrupole splitting (ΔE_Q), quadrupole shift (ε_Q), and hyperfine magnetic field (B_{hf}), provide important information on the electronic density, its symmetry, and magnetic properties at the ^{57}Fe Mössbauer probed nucleus. The method also yields valuable material characteristics from the widths of the spectral lines, their relative intensities, asymmetry of the spectrum, and temperature and field dependence of the hyperfine parameters. The valence and spin states of iron, quantification of nonequivalent Fe sites in the crystal lattice, coordination of Fe in its individual positions, level of ordering and stoichiometry, type of the magnetic ordering, orientation of the

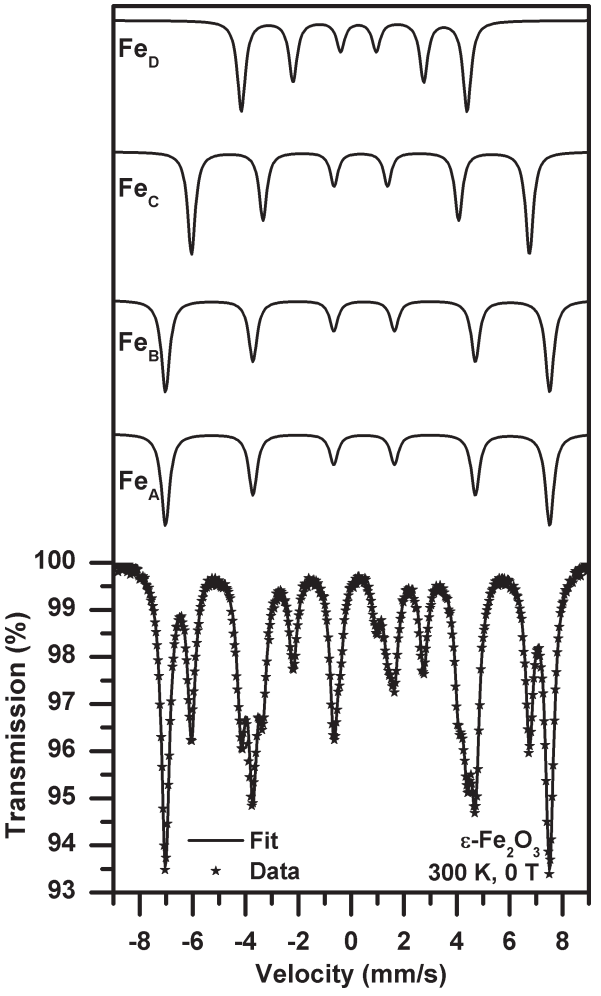

Figure 8. Typical Mössbauer spectrum of the ε-Fe_2O_3 phase recorded at 300 K and without an external magnetic field.

magnetic moments in external magnetic fields (i.e., spin canting and spin frustration), magnetic anisotropy, and magnetic transition temperature represent the principal information that can extracted from the temperature-dependent and in-field Mössbauer spectra.[87,88] In the case of iron(III) oxide polymorphs, ^{57}Fe Mössbauer spectroscopy, applied in a broad range of temperatures and intensities of an external magnetic field, provides a distinct separation of individual spectral components belonging to α-Fe_2O_3, β-Fe_2O_3, γ-Fe_2O_3, and ε-Fe_2O_3, because of different crystal structure and magnetic behavior of these Fe_2O_3 phases reflected in their characteristic temperature- and field-dependent Mössbauer hyperfine parameters.[15]

With respect to the orthorhombic crystal structure of ε-Fe_2O_3 and its Néel temperature of ~490 K, its room-temperature zero-field Mössbauer spectrum consists of four magnetically split components with a ratio of spectral areas of 1:1:1:1 (see Figure 8). This indicates equal ion occupancies at all four crystallographic sites, assuming that all Fe atoms in ε-Fe_2O_3 have the same recoilless fraction. All four sextets exhibit a line intensity ratio of 3:2:1:1:1:2:3 valid for a powdered material with a random distribution of orientations of hyperfine magnetic field (i.e., all possible orientations of the hyperfine magnetic

Table 1. Typical Room-Temperature Mössbauer Hyperfine Parameters of the ε-Fe_2O_3 phase[a]

component	isomer shift, δ (mm/s)	quadrupole splitting, ΔE_Q (mm/s)	hyperfine magnetic field, B_{hf} (T)	relative spectral area of individual spectral components, RA (%)
sextet A−Fe_A	0.37 ± 0.01	−0.25 ± 0.01	44.5 ± 0.3	25 ± 1
sextet B−Fe_B	0.37 ± 0.01	−0.25 ± 0.01	44.6 ± 0.3	25 ± 1
sextet C−Fe_C	0.38 ± 0.01	−0.03 ± 0.01	38.7 ± 0.3	25 ± 1
sextet D−Fe_D	0.23 ± 0.01	−0.15 ± 0.01	25.6 ± 0.3	25 ± 1

[a] The listed isomer shift values are relative to the isomer shift value of α-Fe at room temperature.

field are equally probable within the entire 4π solid angle). However, because of almost the same Mössbauer hyperfine parameters of the two sextets belonging to the magnetic sublattices of A- and B-sites, which implies almost the same local surroundings of Fe atoms situated at the A- and B-sites, the ε-Fe_2O_3 room-temperature overall spectral profile is usually described by three sextets with a ratio of spectral areas of 2:1:1.[24,28,35,39] Contrary to γ-Fe_2O_3 for which, at 300 K and without an applied magnetic field, it is almost impossible to distinguish between the two sextets arising from the tetrahedral and octahedral sites,[81] the separation of the spectral components related to the tetrahedrally and octahedrally coordinated Fe atoms in ε-Fe_2O_3 is clearly evident at 300 K, mainly because of a significantly lower value of the magnetic hyperfine field at the tetrahedral crystallographic positions. For the sake of lucidity, the typical room-temperature Mössbauer hyperfine parameters of ε-Fe_2O_3 are listed in Table 1. The values of the isomer shift for all four sextets fall within the range expected for 6S Fe^{3+} ions in a high-spin state (i.e., $S = 5/2$). The smaller value of δ for sextet D, compared to the δ values for the other three magnetically split components, indicates a tetrahedral coordination of Fe atoms in the structure. The difference between the values of δ for octahedral sextets and tetrahedral sextet of ε-Fe_2O_3 is equal to ∼0.12 mm/s, which fully agrees with that between the tetrahedral sextet and octahedral sextet in γ-Fe_2O_3.[81] A nonzero value of ΔE_Q for sextets A and B implies a slightly distorted surrounding of Fe atoms sitting at the octahedral A- and B-sites, whereas a negligible value of ΔE_Q for sextet C predicates a highly symmetric and undistorted local environment of Fe atoms located at the octahedral C-sites. Based on the value of ΔE_Q for sextet D, the tetrahedral D-sites also exhibit a certain degree of distortion; however, it is not expected to be as pronounced as for the octahedral A- and B-sites (see Table 1). Since the spherically symmetric distribution of the electronic charge for Fe^{3+} ions results in zero contributions of the orbital and dipolar magnetic hyperfine fields, the overall hyperfine magnetic field is then determined only by a negative Fermi contact term, which is oppositely oriented, with respect to the magnetic moment of the Fe^{3+} ion. In this case, the hyperfine magnetic field of the Fe^{3+} ion at a particular site is directly proportional to the magnetization at the sublattice to which this Fe^{3+} ion belongs. The values of the hyperfine magnetic fields corresponding to individual spectral components of ε-Fe_2O_3 thus reflect the sublattice magnetizations at particular sites at a given temperature.[89] Therefore, in correspondence with the results of neutron diffraction experiments and molecular field theory study, both providing information on the magnitude of magnetic moments of Fe atoms at different crystallographic sites of ε-Fe_2O_3 (see section 3),[29,34,36] sextets A and B exhibit the same value of B_{hf}, which is somewhat higher than that observed for sextet C, and sextet D shows the lowest B_{hf} value of all of the magnetically split components.

As the temperature is reduced, the zero-field Mössbauer spectrum of ε-Fe_2O_3 retains its features down to 150 K, below which a radical change in its spectral profile is observed. The analysis of low-temperature Mössbauer spectra shows that, between 150 K and 80 K, most of the hyperfine parameters of various Fe sites deviate from the thermal dependences displayed at higher temperatures. These anomalies particularly involve the tetrahedral sites in the structure of ε-Fe_2O_3, for which a 20% increase in B_{hf} (∼9 T) is registered between 140 K and 100 K, accompanied by a shift in both the isomer shift and the quadrupole splitting in the same temperature range (see Figure 9). As the $\Delta E_{Q,A}$ parameter of sextet A changes its sign from a negative value to a positive value and δ_A unusually decreases within this temperature range, Gich et al.[36] guessed that, upon cooling the ε-Fe_2O_3 sample below 150 K, some structural changes may affect the A-site coordination octahedron, which, subsequently, may induce some changes in the coordination of the D-sites reflected in the value and the sign of $\Delta E_{Q,D}$ (see Figure 9). In addition, spin reorientations should also be taken into account to play some role in the micromagnetic state of ε-Fe_2O_3 between 150 K and 80 K as they commonly manifest themselves by significant changes in the quadrupole splitting parameter. For example, this happens at the Morin transition temperature (T_M) in α-Fe_2O_3 (at ∼265 K for bulk α-Fe_2O_3), at which the transition from a high-temperature weakly ferromagnetic state to a low-temperature antiferromagnetic state, triggered by a 90° spin reorientation phenomenon, is observed.[15,90,91] Above T_M, the magnetic moments of Fe^{3+} ions lie in the basal plane of the crystallographic structure of α-Fe_2O_3 and are coupled in an antiferromagnetic manner across the shared FeO_6 octahedron faces along the *c*-axis. In the basal plane, two interpenetrating antiferromagnetic sublattices are recognized. However, the atomic magnetic moments of these two sublattices are not exactly antiparallel and are rotated by a small angle around the α-Fe_2O_3 [001]-axis (i.e., are spin canted), giving rise to a weak magnetic moment along the *c*-axis, because of the Dzyaloshinsky−Moriya antisymmetric interaction.[91−93] Below T_M, the atomic magnetic moments of one sublattice are perfectly antiparallel to those of the other sublattice, constituting pure antiferromagnetic ordering with an antiferromagnetic axis being parallel to the α-Fe_2O_3 [001]-axis. The Morin transition in α-Fe_2O_3 is then accompanied by a change in the value of the ΔE_Q parameter from 0.20 mm/s for the weakly ferromagnetic state

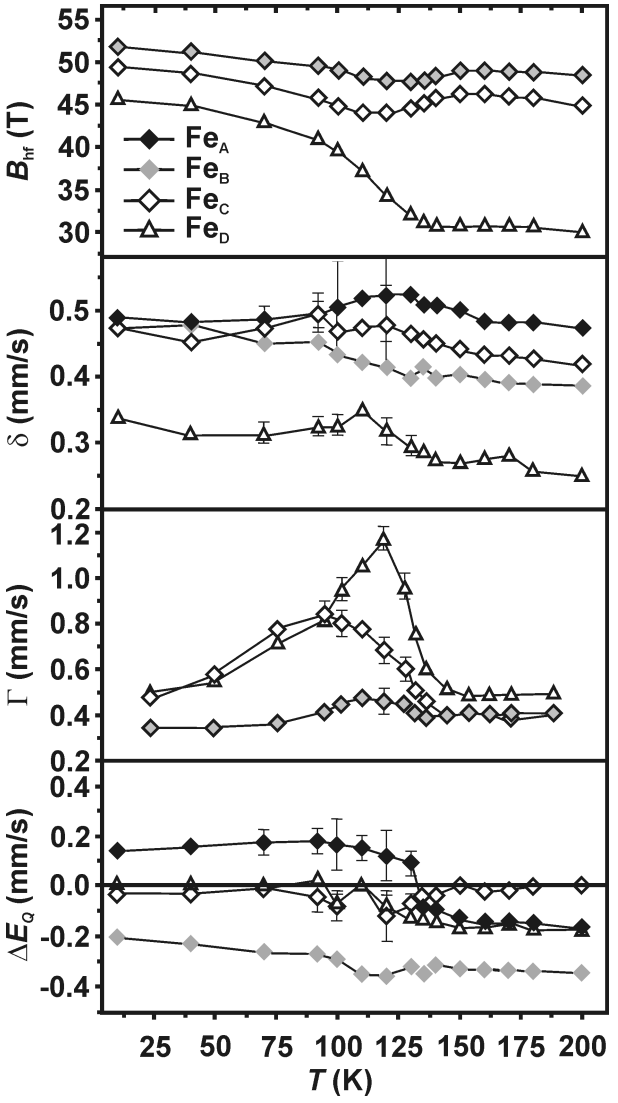

Figure 9. Temperature dependence of hyperfine parameters of the ε-Fe_2O_3 phase derived from its Mössbauer spectra recorded at various temperatures. (Adapted from Gich et al.[29])

to −0.40 mm/s for the antiferromagnetic state.[15,94] Thus, the structural transformations and possible spin reorientation effects, taking place in the temperature interval from 150 K down to 80 K, lead to a significant magnetic softening of ε-Fe_2O_3. The changes in ΔE_Q for sextets A and D can be associated with an experimentally confirmed weakening of the spin−orbit coupling of Fe cations (via diminution of the orbital component of the overall Fe^{3+} magnetic moment), which has a direct impact on the magnetic anisotropy of ε-Fe_2O_3.[50] The fact that the transition from one magnetic regime to another is rather broad and is accompanied by a coexistence of several magnetically different phases between 80 K and 150 K is further documented by line width parameters that increase for all magnetically split components below 150 K (see Figure 9). The line broadening is more pronounced in the case of sextet D, which fortifies the hypothesis of emergence of some disorder at the crystallographically different sites of ε-Fe_2O_3 structure. Hence, the changes in all Mössbauer hyperfine parameters of all four sextets, including their substantial line broadening in the temperature range from 150 K down to 80 K, suggest a redistribution of electronic density in the local surrounding of the probed Fe^{3+} ions and a change of geometry of the iron sites in the structure of ε-Fe_2O_3 accompanied likely by spin reorientation phenomena.[28,29,33,35]

Below 80 K, in most cases, only two sextets are resolved in the Mössbauer spectrum of ε-Fe_2O_3: the first one arises from the three different octahedral sites and the second one belongs to the tetrahedral sites. At 4.2 K, the analysis of the octahedral sextet gives $\delta_O \approx 0.49$ mm/s, $\Delta E_{Q,O} \approx 0$ mm/s, and $B_{hf,O} \approx 51.6$ T, whereas, for the tetrahedral sextet, we find $\delta_T \approx 0.31$ mm/s, $\Delta E_{Q,T} \approx 0$ mm/s, and $B_{hf,T} \approx 45.8$ T.[33] Note that the value of B_{hf} for the tetrahedral sites is much smaller than that reported for tetrahedral positions in the structure of bulk γ-Fe_2O_3 ($B_{hf} \approx 52.0$ T at 4.2 K). The temperature dependence of the hyperfine magnetic field at individual sites of ε-Fe_2O_3, derived from the measured Mössbauer spectra, shows that, for the distorted octahedral sites, the temperature behavior of B_{hf} is governed by the Brillouin function with $S = 5/2$, whereas the Langevin function seems to be correct for a description of the temperature evolution of the hyperfine magnetic field at the regular octahedral and tetrahedral sites. Thus, it follows that, within the time scale of the Mössbauer technique ($\sim 10^{-8}$ s), the magnetic moments of the Fe^{3+} ions situated at the A- and B-sites behave as quantum spins, contrary to the magnetic moments of the Fe atoms located at the C- and D-sites, which behave as freely rotating classical spins.[33]

It turns out that if ε-Fe_2O_3 is exposed to an external magnetic field, the measured in-field Mössbauer spectrum then brings a deeper insight for understanding its magnetic state. In general, in-field ^{57}Fe Mössbauer spectroscopy allows one to investigate the arrangement of the atomic magnetic moments within the sample effectively and is considered as a key experimental technique in the study of unusual phenomena (i.e., spin canting, spin frustration, spin-glass-like state of nanoparticle surface atomic magnetic moments, etc.)[81,95−98] that appear in particles with sizes of units or tens of nanometers. In addition, the separation of individual spectral contributions in an applied magnetic field enables one to determine the magnetic structure of the studied material (i.e., different crystallographic sites establishing different magnetic sublattices)[88,89,99] and/or quantify the portions of impurity phases that have very similar zero-field Mössbauer hyperfine parameters and are therefore undistinguishable in zero-field Mössbauer spectra. In the presence of an external magnetic field, the effective hyperfine magnetic field ($\boldsymbol{B}_{eff}$) at the ^{57}Fe nucleus is expressed as a vector sum of the hyperfine magnetic field ($\boldsymbol{B}_{hf}$) and the external magnetic field ($\boldsymbol{B}_{ext}$), i.e., $\boldsymbol{B}_{eff} = \boldsymbol{B}_{hf} + \boldsymbol{B}_{ext}$. The effective hyperfine magnetic field is inclined at an angle θ to the γ-ray direction. It follows that $B_{hf}^2 = B_{eff}^2 + B_{ext}^2 - 2B_{eff}B_{ext}\cos(\theta)$. If $B_{hf} \gg B_{ext}$, B_{eff} and B_{ext} are practically collinear and $B_{eff} \approx B_{hf} + B_{ext}\cos(\theta)$. Because ε-Fe_2O_3 is composed of Fe^{3+} ions, the direction of the hyperfine magnetic field is antiparallel to the orientation of the magnetic moment of the Fe^{3+} ion,

as a result of the negative Fermi contact term. The areas of the lines in a sextet are then in the ratio of 3:x:1:1:x:3, with $x = 4\sin^2(\theta)/[1 + \cos^2(\theta)]$.[87] In an experimental geometry when the applied magnetic field points in the direction of γ-ray propagation, $x = 0$ if the alignment of magnetic moments is parallel or antiparallel, with respect to the direction of the applied magnetic field (i.e., ferromagnetic and ferrimagnetic materials of a powder, polycrystalline, and monocrystalline form with a dominant magnetic dipolar hyperfine interaction and an absence of the internal texture), and $x = 4$ for a perpendicular orientation of magnetic moments to the direction of the external magnetic field (i.e., antiferromagnetic materials of monocrystalline form with a dominant magnetic dipolar hyperfine interaction, an absence of the internal texture, and for the case of the external magnetic field oriented along the characteristic antiferromagnetic axis and with a magnetic induction higher that the characteristic spin-flop field of the given antiferromagnetic material).[100] To determine the angle θ (i.e., the orientation of B_{hf} at a particular Fe site, with respect to the direction of incoming γ-rays and external magnetic field), it is then easy to show that $\theta = \arcsin\{[6r/(4 + 3r)]^{1/2}\}$, with $r = A_{2,5}/A_{1,6}$, where $A_{1,6}$ is the spectral area of the first and sixth sextet lines ($A_{1,6} = 3$) and $A_{2,5}$ is the spectral area of the second and fifth sextet lines.

The in-field Mössbauer spectrum of ε-Fe_2O_3 shows that the effective hyperfine magnetic field increases for the A- and D-sites, while it decreases for the B- and C-sites compared to the values of respective hyperfine magnetic fields at particular sites. Analyzing the pioneering in-field Mössbauer spectrum of ε-Fe_2O_3 at 9 K and under an external magnetic field of 6 T, applied parallel to the direction of the γ-rays,[24] it was deduced that the hyperfine magnetic field at the octahedral A-sites is canted by ~35° from the orientation of B_{ext} (see Figure 10). The hyperfine magnetic fields at the octahedral B- and C-sites were found to be parallel to each other and were canted in the opposite direction by approximately the same angle (~144°). Finally, the hyperfine magnetic field at the tetrahedral D-sites displayed canting at ~65° from the orientation of B_{ext}. Thus, a ferrimagnetic structural arrangement with three (or four) sublattices was proposed, which gives a net magnetization of ~0.4 μ_B per Fe (taking into account a value of 5 μ_B for the 6S Fe^{3+} ion). Later refinements, based on the analyses of in-field Mössbauer spectra measured in the temperature range from 9 K to 250 K and under an applied magnetic field of 6 T, show that ε-Fe_2O_3 behaves as a collinear ferrimagnetic material with two magnetic sublattices, i.e., A = Fe_A + Fe_D and B = Fe_B + Fe_C, which are canted symmetrically or antiparallel with incomplete alignment.[33] The fact that the magnetic moments of Fe^{3+} ions at the C- and D-sites obey a Langevin-like behavior is associated with the existence of multiple spin states, because of competing superexchange interactions and possibly dipolar interactions. The in-field Mössbauer data indicate that the spin structure of ε-Fe_2O_3 is mainly driven by strong antiferromagnetic superexchange interactions that occur between Fe_A and Fe_B ions. The magnetic moments of Fe^{3+} ions at the A- and C-sites interact with each other in a similar way, but the corresponding superexchange interaction are not as strong as in the case of Fe_A-Fe_B interaction. Thus, the magnetic moments of Fe_C ions become more affected by intrasublattice interactions than Fe_A and Fe_B ions. The topology thus causes frustration for both superexchange and dipolar interactions, which induces spin disorder at the octahedral C-sites. The orientation of Fe_D ions is governed by an intersublattice magnetic coupling, but the results imply that all the antiferromagnetic interactions between an Fe_D ion and its seven $Fe_{B,C}$ neighbors cannot be energetically satisfied simultaneously.[33]

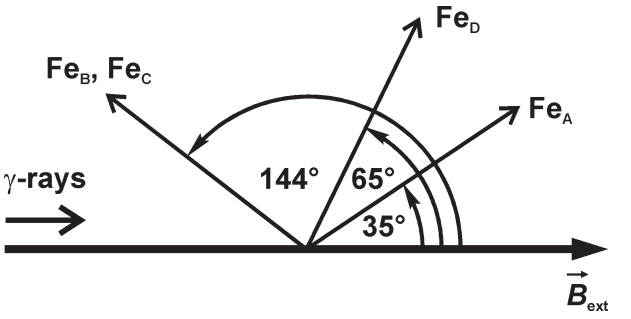

Figure 10. Schematic representation of the orientation of the hyperfine magnetic fields in the ε-Fe_2O_3 phase, derived from its in-field Mössbauer spectrum collected at 9 K and under an external magnetic field of 6 T applied along the direction of propagation of γ-rays. (Adapted from Tronc et al.[24])

A rather different explanation of the ground magnetic state of ε-Fe_2O_3 has been proposed by Rehspringer et al.[35] The in-field Mössbauer spectra of ε-Fe_2O_3, measured at 4.2, 120, and 160 K under an external magnetic field of 5 T applied perpendicular to the direction of γ-rays, again indicate two magnetic sublattices (but this time, A = Fe_A + Fe_B and B = Fe_C + Fe_D). At 160 K, the magnetic moments of the two sublattices are antiparallel to each other and are collinear with the applied magnetic field. However, at 4.2 K, an external magnetic field causes the magnetic moments of the (Fe_C + Fe_D) sublattice to orient almost perpendicular to its direction. These results were then explained in terms of different magnetic anisotropy of the ε-Fe_2O_3 at 160 and 4.2 K. Because of the weak magnetic anisotropy at 4.2 K and the possible presence of a low-temperature metamagnetic state (see section 5), the magnetic moments that belong to one sublattice are easily flopped under the external magnetic field, whereas above 120 K, the magnetic structure of ε-Fe_2O_3 resembles characteristics of a collinear 2-sublattice antiferromagnet driven by strong magnetic anisotropy.[35]

5. Magnetization Measurements of the ε-Fe_2O_3 Phase

While zero-field and in-field ^{57}Fe Mössbauer spectroscopy gives information on the local magnetic properties of the probed Fe atoms, data from the magnetization measurements report on the macroscopic magnetic properties of the investigated samples. Similar to that indicated by the analyses of the zero-field and in-field temperature-dependent Mössbauer spectra of ε-Fe_2O_3, the interpretation of the magnetization measurements

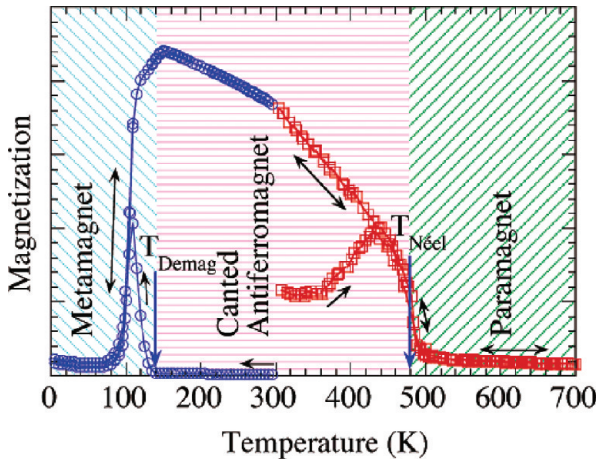

Figure 11. Proposed magnetic regimes of the ε-Fe_2O_3 phase at various temperatures. (Adapted from Kurmoo et al.[28])

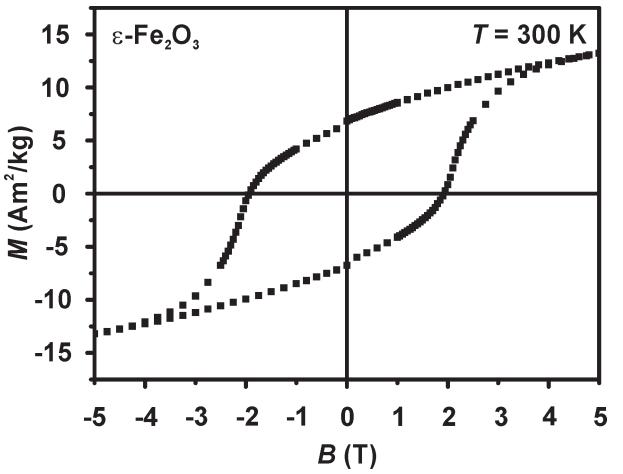

Figure 12. Typical room-temperature hysteresis loop (M vs B dependence) of the ε-Fe_2O_3 phase. (Adapted from Jin et al.[16])

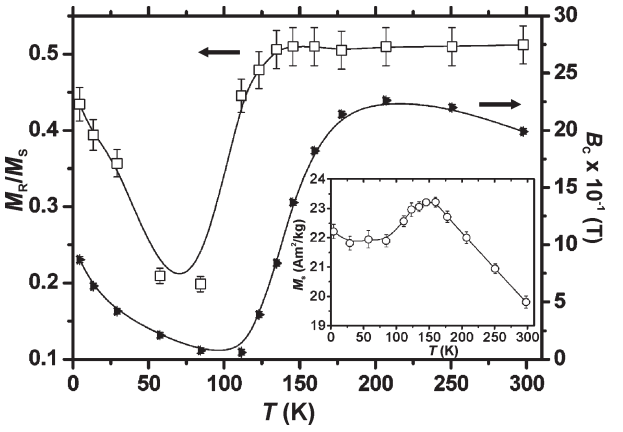

Figure 13. Temperature evolution of the coercivity (B_C) and squareness ratio (M_R/M_S) of the ε-Fe_2O_3 phase. (Adapted from Gich et al.[29])

suggests two possible ground magnetic states of ε-Fe_2O_3. Thus, ε-Fe_2O_3 behaves either as a collinear ferrimagnet with a transition to the square-wave incommensurate magnetic structure at low temperatures[16,24,29,33,34] or as a canted antiferromagnet characterized by differently canted antiferromagnetic states with a sign of transition to a metamagnetic state at low temperatures (see Figure 11).[28,35]

Generally, ε-Fe_2O_3 displays complex magnetic properties that dramatically change at two significant temperatures, namely, at ~490 K and ~110 K. At ~490 K, ε-Fe_2O_3 passes from a paramagnetic state to a magnetically ordered state. As the temperature decreases, the coercivity of ε-Fe_2O_3 rapidly increases, reaching a value of ~2 T at room temperature (see Figure 12).[16,29] The magnetic hardness of ε-Fe_2O_3 then first increases slightly when the temperature decreases from 300 K to 200 K (~2.2 T at 200 K), then it drastically decreases to zero at ~100 K, and finally, it again strengthens down to 2 K (see Figure 13).[29] Such a large change in the magnetic hardness of ε-Fe_2O_3 reflects a change in the magnetocrystalline anisotropy, which may result from either a change in the geometry of the Fe sites in the crystal structure and/or a reorientation phenomenon of the Fe^{3+} magnetic moments, as reported for α-Fe_2O_3.[29,36,37,50] Furthermore, the collapse in B_C is accompanied by a decrease in the squareness ratio (M_R/M_S, where M_R is the remanent magnetization) (see Figure 13). The temperature-dependent magnetization curves, recorded upon warming and cooling ε-Fe_2O_3 in the same external magnetic field, show two anomalies, i.e., a sharp change of the slope at ~110 K below which the magnetization abruptly decreases, and a weak change at ~150 K, where a maximum in the magnetization is observed (see Figure 14). According to some research groups, the unusual behavior of magnetization of ε-Fe_2O_3 at ~110 K, which has not been registered in the $GaFeO_3$ and $AlFeO_3$ isomorphous systems, is ascribed to the transition from one canted antiferromagnetic state (characterized by a certain canting angle) to another canted antiferromagnetic state with a smaller resultant magnetic moment (i.e., with a smaller canting angle).[28] This transition, which is sometimes referred to as a Morin-like transition, is also evidenced by sharp peaks (centered at ~110 K) appearing in both the real and imaginary components of the AC susceptibility, which is attributed to a change in the magnetic hardness of this peculiar magnetic material. However, with increasing frequency of the applied magnetic field, the maxima in the AC-susceptibility parts shift to lower temperatures, in contrast to the response of spin glasses, single molecule magnets, and an assembly of superparamagnetic particles. Moreover, the magnetization curves upon warming and subsequent cooling exhibit irreversibility below 110 K if the temperature dependence of magnetization is measured in a relatively small applied magnetic field (from ~0.5 mT to ~0.1 T). Some authors claim that the presence of this bifurcation point between magnetization curves under warming and cooling conditions can be regarded as a mirror image of the transition associated with a paramagnetic−ferrimagnetic transition of a hard magnet.[28] As the intensity of the applied magnetic field increases, the separation between warmed and cooled magnetization curves progressively diminishes and the curves become identical when recorded under an external magnetic field of >2 T. This suggests a possible presence of a metamagnetic transition at ~50 K with a critical field (field required to change the orientations of the magnetic moments) lying between 0.1 T and 1 T and

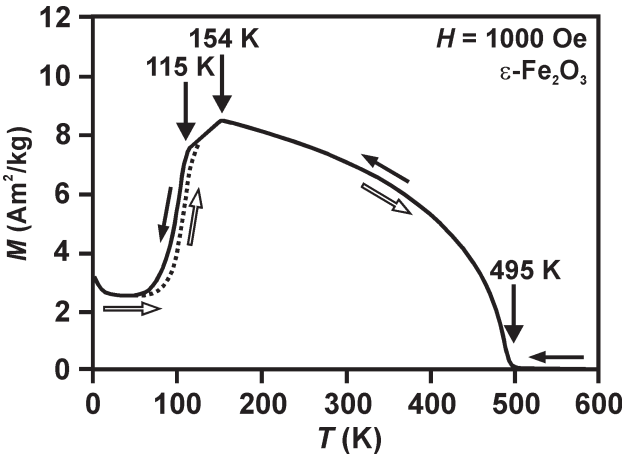

Figure 14. Temperature dependence of magnetization (M) of the ε-Fe_2O_3 phase upon cooling and subsequent warming. (Adapted from Sakurai et al.[37])

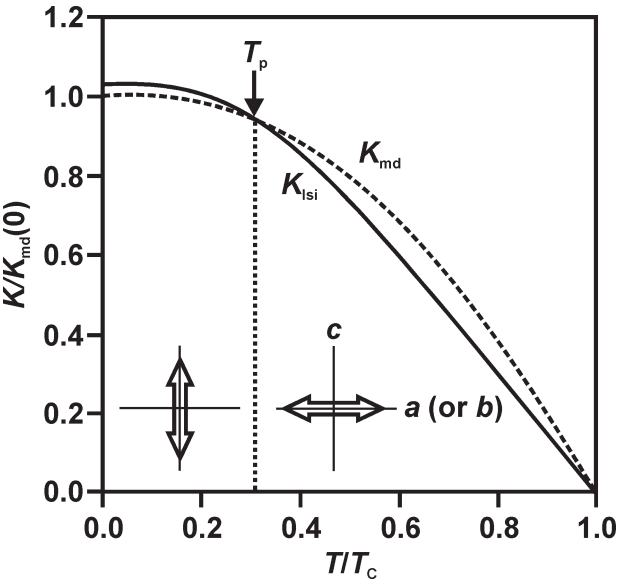

Figure 15. Calculated temperature dependences of magnetic anisotropy constants derived from magnetic dipole−dipole interaction (represented by K_{md}) and local single-ion anisotropy (represented by K_{lsi}). (Adapted from Sakurai et al.[37])

powered probably by the temperature dependence of the anisotropy field increasing at low temperatures.[28]

The room-temperature canted antiferromagnetic state of ε-Fe_2O_3 is further documented by an almost linear dependence of the magnetization with the applied magnetic field, its nonsaturation at high external magnetic fields (typically 5−7 T), and low magnetization values exhibited under 5 T.[35] This has been supported in terms of an analysis of values of distances and angles between Fe atoms sitting at four different crystallographic sites of the ε-Fe_2O_3 crystal structure.[28] It turns out that intrasublattice Fe_D-Fe_D magnetic interactions, which are supposed to be of an antiferromagnetic nature, are responsible for a frustration induced between ferromagnetic $Fe_A-Fe_B-Fe_C$ units establishing an overall antiferromagnetic ground state of ε-Fe_2O_3 at room temperature. The canting then probably arises as a consequence of this frustration, given the absence of the single-ion anisotropy.

To decide whether the transition at ~110 K exhibits the features of the Morin transition as partly predicated by Mössbauer spectroscopy results, a theoretical analysis has been presented by Sakurai et al.,[37] taking into account the temperature behavior of relevant contributions to the magnetic anisotropy of the system. In the case of α-Fe_2O_3, it is known that the Morin transition, resembling characteristics of the first-order thermodynamic transition, is driven by an energy competition between a strong magnetic dipolar anisotropy (favoring the orientation of spins in the basal plane of α-Fe_2O_3 crystal structure) and local single-ion anisotropy (originating from a spin−orbital interaction and favoring the orientation of spins in the (111) plane of the α-Fe_2O_3 crystal structure) with different temperature dependencies. At T_M, the magnetic dipolar anisotropy is equal to the local single-ion anisotropy which leads to the change in the sign of the total magnetocrystalline anisotropy, and a 90° spin-flop occurs, accompanied by a change in the easy axis of the magnetic anisotropy.[91] Therefore, a similar mechanism has been used to explain the observed phase transition in ε-Fe_2O_3. Within this approach, the magnetic anisotropy energy (E_{MA}) of ε-Fe_2O_3 is taken as the sum of the energy of the magnetic dipole−dipole interaction anisotropy (E_{MD}) and the local single-ion anisotropy (E_{lsi}), i.e.,

$$E_{MA} = E_{md} + E_{lsi}$$

when the directions of the magnetic dipole−dipole interaction anisotropy and local single-ion anisotropy are assumed to be perpendicular and parallel to the c-axis, respectively. Thus, one can write that $E_{md} = K_{md}\cos^2(\varphi)$ and $E_{lsi} = K_{lsi}\sin^2(\varphi)$, where K_{md} and K_{lsi} are the corresponding magnetic anisotropy constants and φ represents the angle between the c-axis and the spin direction. It is then shown that, when the ratio of K_{lsi} to K_{md} is 1.03 at 0 K, the calculated curves of the temperature dependences of K_{lsi} and K_{md} cross at ~150 K (see Figure 15). At this point of intersection of the K_{lsi} and K_{md} curves, the phenomenon of spin reorientation occurs, because of the change in the easy axis from the a-axis (or b-axis) to the c-axis. In terms of this model and its results, experimentally reported anomalous temperature behavior of the magnetization and coercivity of ε-Fe_2O_3 can be explained. For example, a gentle decrease in the magnetization below ~150 K can be understood as a 90° rotation of the easy axis and the strange decrease in the coercive field below ~150 K can be interpreted by the disappearance of the magnetic anisotropy due to the compensation between E_{md} and E_{lsi}. Thus, according to this theoretical study, the spin reorientation seems to be happening, along with the magnetic transition occurring at ~110 K, having attributes of the Morin transition, as observed in α-Fe_2O_3.[37]

However, as previously mentioned, there have been numerous works establishing other ground magnetic states of ε-Fe_2O_3. The first detailed structural and Mössbauer study on ε-Fe_2O_3, carried out by Tronc et al.,[24] found it to be a 4-sublattice ferrimagnetic material, the magnetic behavior of which is governed by three types of Fe−O−Fe bonds in the structure. These bonds

include the following: (i) strong antiferromagnetic bonds at an angle close to 180°; (ii) bonds at an angle close to 120°, which are also antiferromagnetic but not as strong as the close-to-180° bonds; and (iii) bonds at the angle close to 90°, which are only weakly magnetic. The analysis shows that the ferrimagnetic response of ε-Fe_2O_3 is driven by strong antiferromagnetic coupling between octahedral Fe_A and (Fe_B, Fe_C) ions and frustrated antiferromagnetic interactions involving tetrahedral Fe_D ions. Moreover, the magnetic moments of Fe^{3+} ions, located at the tetrahedral D-sites, undergo dynamical phenomena, because of weak magnetic coupling with their adjoining magnetic partners, partly affecting the magnetic moments of Fe^{3+} ions situated at the regular octahedral C-sites. Thus, three magnetic sublattices, arising from different octahedral sites, exhibit an almost-collinear ferrimagnetic ordering of Fe^{3+} magnetic moments, whereas a lack of alignment, together with possible disorder, is expected at the tetrahedral sites.

Gich et al.[29] have recently supported the idea of a ferrimagnetic structure of ε-Fe_2O_3 and consequently clarified what happens to magnetic moments of Fe^{3+} ions when ε-Fe_2O_3 is cooled. They have proposed that, at room temperature, ε-Fe_2O_3 behaves as a collinear ferrimagnet with the Fe^{3+} magnetic moments oriented along the *a*-axis and a net magnetization originating from the small magnetic moment of Fe^{3+} ions occupying tetrahedral sites. The room-temperature saturation magnetization for the ε-Fe_2O_3 phase is found to be equal to ~20 A m^2/kg (~0.29 μ_B/Fe^{3+} ion, in accordance with the value derived from the room-temperature neutron diffraction data and the Mössbauer spectrum). Since the expected moment for Fe^{3+} ions should be 5 μ_B, it is regarded as evidence that ε-Fe_2O_3 is ferrimagnetic at room temperature. The magnetic structure remains ferrimagnetic down to 150 K, below which temperature a series of magnetic and structural transformations occur, terminating at ~80 K when ε-Fe_2O_3 enters into a low-temperature magnetic state characterized by a square-wave incommensurate magnetic structure having reduced coercivity and a smaller magnetization, compared to the high-temperature ferrimagnetic regime. The transition between these two magnetic states is not sharp and proceeds over a broad temperature interval, implying its complexity. The measurements of zero-field-cooled (i.e., ZFC) and field-cooled (i.e., FC) magnetization curves at low applied magnetic fields (typically ≤0.1 T) show irreversibility between them at < 100 K, contrary to the reversibility reported at > 100 K. When heating from low temperatures, the ZFC magnetization curve of ε-Fe_2O_3 exhibits a significant increase when the temperature increases from ~80 K to ~150 K, indicating three consecutive stages. According to the magnetization results, and, in agreement with neutron powder diffraction and Mössbauer analyses, Gich et al.[36] claimed that between 150 K and 110 K, a second-order structural transition, presumably powered by changes in the coordination of Fe_A and Fe_D sites, occurs simultaneously with the emergence of an incommensurate magnetic order. The magnetic structure then undergoes several transformations as the temperature is further decreased, but no additional changes are observed at < 80 K. These structural and magnetic transformations weaken the magnetic anisotropy, resulting in an extraordinary magnetic softening of ε-Fe_2O_3 at < 150 K. As the large room-temperature coercivity is again retrieved after warming ε-Fe_2O_3 back to 300 K, it is suggested that the bizarre decrease in the coercive field is most probably connected with the decrease in the magnetocrystalline anisotropy constant. In this context, Gich et al.[36] have noted that a strong weakening in the magnetocrystalline anisotropy can be understood in terms of the transition from the single-domain to an inhomogeneous magnetization state, as evidenced by a decrease in the squareness (M_R/M_S) ratio from 0.50 at 300 K to 0.20 at 80 K (see Figure 13). The decline in coercivity has been then ascribed to the loss of the single-domain character of ε-Fe_2O_3 at low temperatures and the Arrhenius nature of domain wall motion. At high temperatures, the size of ε-Fe_2O_3 nanoparticles ($d_{\varepsilon\text{-}Fe_2O_3}$) is smaller than the critical size for the single-domain state (d_{SD}). Upon reducing the temperature, the magnetocrystalline anisotropy constant (K_{MC}) of ε-Fe_2O_3 nanoparticles decreases, which is reflected in a reduction of the critical single-domain size, as d_{SD} is dependent on K_{MC} (for spherical nanoparticles, $d_{SD} \propto K_{MC}^{1/2}$). As $d_{\varepsilon\text{-}Fe_2O_3} > d_{SD}$ at low temperatures, ε-Fe_2O_3 nanoparticles are not single-domain any longer. In addition, the decrease in K_{MC} provokes an increase in the width of the domain wall. Thus, according to Gich et al.,[36] if the width of the domain wall becomes larger than the size of an ε-Fe_2O_3 nanoparticle with a sufficiently low K_{MC}, the particle magnetization is expected to enter into an extended inhomogeneous state known as a "vortex state". In addition, as already discussed, the decrease in K_{MC} (and resultant collapse in B_C) is a consequence of a strong reduction in the spin−orbit coupling documented by a dramatic decrease in m_{orb} between 150 K and 120 K (see Figure 6). The recent study by Tseng et al.[50] claimed that, taking into account the anomalous behavior of the δ and ΔE_Q parameters for the Fe_A and Fe_D sites in the temperature interval from ~110 K to ~160 K (see Figure 9), this weakening of spin−orbit coupling arises from the reduction in the electron transfer between Fe and O ions for the Fe_A and Fe_D sites, resulting in an increase in ionicity of some Fe−O−Fe bonds (especially those between the Fe_A and Fe_D ions). After warming the ε-Fe_2O_3 phase back through the transition at ~110 K, the spin−orbit coupling retains its strength, indicating nonmonotonic behavior of the Fe−O bond lengths. Assuming that the lattice distortions are governed by changes in the magnetic structure in the course of the gradual magnetic transition, Tseng et al.[50] qualitatively understood the re-entrant behavior of the orbital magnetic moment and, consequently, spin−orbit coupling, in terms of the effect of lattice distortions on m_{orb} reduction and the resultant impossibility to stabilize these distortions.

From the viewpoint of a perspective application of ε-Fe_2O_3, the search for a mechanism that yields a giant room-temperature coercivity of ε-Fe_2O_3 has been the scope of several research works. Such a large room-temperature coercive field of ε-Fe_2O_3 is rather surprising and cannot be solely caused by symmetric 6S Fe^{3+} ions

with a half-filled d-shell, in contrast to cobalt-containing materials, where a large coercivity is, in most cases, invoked by highly anisotropic Co ions.[101,102] One explanation, proposed by Kurmoo et al.,[28] sees defects playing an essential role on the magnetic hardness of ε-Fe_2O_3. The presence of defects is promoted by the crystal structure of ε-Fe_2O_3, which belongs to a polar group. It is then supposed that the defect induces two possible orientations within a crystallite, thus enhancing the magnetocrystalline anisotropy of the ε-Fe_2O_3 nanoparticle. In this context, any contributions from the multidomain behavior of the ε-Fe_2O_3 nanoparticle and strong dipolar interparticle interactions are strictly excluded as the former phenomenon does not, with the highest probability, occur at room temperature and the latter effect would not be so powerful to influence the magnetic anisotropy of every ε-Fe_2O_3 nanoparticle in the system. On the other hand, a hypothesis, raised by Jin et al.,[16,41] has identified other factors that seem to be crucial for achieving such a high room-temperature coercivity in ε-Fe_2O_3. Since B_C is generally dependent on the magnetocrystalline anisotropy and saturation magnetization (i.e., $B_C \propto K_{MC}/M_S$),[54] the single-domain character of ε-Fe_2O_3 nanoparticles, evoking high magnetic anisotropy ($K_{MC} \approx 2 \times 10^5$ J/m^3), and low values of magnetization ($\approx$ 15 A m^2/kg) observed at high applied magnetic fields are considered to shape the resultant giant B_C of ε-Fe_2O_3. Note that, among the polymorphs of Fe_2O_3, ε-Fe_2O_3 exhibits the highest value of K_{MC}, compared to α-Fe_2O_3 (which has a K_{MC} value of $\sim 10^4$ J/m^3) and γ-Fe_2O_3 (which has a K_{MC} value of $\sim 10^3$ J/m^3).

A rather different explanation why the ε-Fe_2O_3 phase possesses such a high coercive field at room temperature has been presented by Tseng et al.[50] Based on the analyses of experimental data from X-ray magnetic circular dichroism and application of sum-rules calculations, which allows one to separate the orbital (m_{orb}) and spin (m_{spin}) components of the magnetic moment (see Figure 6), they identified the m_{orb} value of Fe^{3+} magnetic moment, having a significantly high value, being responsible for a large magnetocrystalline anisotropy and, consequently, a giant room-temperature coercivity. As the nonzero value of m_{orb} is quite unexpected in the case of a half-filled $3d^5$ electronic state of Fe^{3+} ion (for $3d^5$ configuration, we expect the angular momentum (L) to be equal to zero), its origin is connected with distortions of Fe^{3+} coordination polyhedra observed for the two different octahedral sites (i.e., the Fe_A and Fe_B sites; see section 3) and the tetrahedral sites (i.e., the Fe_D sites; see section 3) in the crystal structure of the iron(III) oxide ε-polymorph. According to Tseng et al.,[50] the distortions of Fe sites then lead to Fe(3d)−O(2p) mixing and O(2p)-to-Fe(3d) charge transfer, which, along with the crystal-field effects, lifts the electronic degeneracy and causes the occurrence of nonzero m_{orb} values for the ε-Fe_2O_3 phase, in contrast to the case of other iron oxides, where $m_{orb} \approx 0$, because of their crystalline symmetry. Considering the similar distortion-induced behavior of the m_{orb} value reported for $GaFeO_3$, which is isostructural to ε-Fe_2O_3, the authors claim that, because of the off-center displacement of Fe^{3+} ions along the c- and b-axis, resulting in broken orbital parity symmetries, the largest orbital magnetic moment is expected to be along the a-axis. Because of the emergence of spin−orbit coupling caused by nonzero m_{orb} values, the a-axis then becomes the magnetic easy axis along which the magnetic moments of Fe^{3+} ions that occupy various nonequivalent crystallographic sites lie. Because the directions of the magnetic moments are very firmly coupled to this axis, the magnetocrystalline anisotropy gets larger, thus stemming from a significantly large spin−orbit coupling phenomenon. In addition, as noted by Tseng et al.,[50] the confirmed existence of large spin−orbit coupling would clarify the question of why magnetic and dielectric properties of ε-Fe_2O_3 are strongly coupled (see section 6).[17]

In principle, the value of the room-temperature coercivity of ε-Fe_2O_3 is strongly dependent on the size, size distribution, morphology, and degree of cation substitution of ε-Fe_2O_3 nanoobjects. A recently performed study shows that the room-temperature coercive field can be enlarged if the ε-Fe_2O_3 nanoparticles are not spherical. For rodlike ε-Fe_2O_3 nanoparticles embedded in a SiO_2 matrix, which have been oriented by an external magnetic field ($B_{ext,s}$) during the synthetic procedure, the coercive field reaches a value of $\sim$2.34 T at 300 K if a value of $B_{ext,s}$ = 2 T has been applied along the z-axis of the respective matrix crystal for 24 h.[51] Taking into account a magnetic rotation process governed by solely uniaxial magnetic anisotropy, subsequent simulation calculation of the room-temperature hysteresis loop suggests that, for a perfectly oriented ε-Fe_2O_3 nanorod, the coercive field may become as large as 4.1 T.

In the case of ε-Fe_2O_3 in the form of thin films, the value of the room-temperature coercive field has been reported to be equal to $\sim$0.8 T, which is smaller than the value of $\sim$2 T that has been observed for ε-Fe_2O_3 nanoparticles. Nevertheless, even such room-temperature coercivity, in combination with the film nature of ε-Fe_2O_3, is still appealing for its application in future spintronic devices, taking into account its magnetoelectric behavior (see section 6).[53]

If some of the Fe^{3+} ions are replaced by other elements, the magnetic properties of the resulting doped ε-Fe_2O_3 phase are affected, depending on the nature and degree of substitution of foreign ions. So far, the effects of Ga^{3+}, Al^{3+}, and In^{3+} doping on a magnetic response of substituted ε-Fe_2O_3 analogs have been investigated.[65,66,85,86] As already mentioned previously, increasing the concentration of Ga^{3+}, Al^{3+}, and In^{3+} ions in the crystal structure of the ε-Fe_2O_3 phase leads to a progressive decrease in the T_C and B_C(300 K) values, compared to those reported for undoped ε-Fe_2O_3.[65,66,85] In the case of Al^{3+} substituting ions in the studied concentration range (i.e., ε-$Al_xFe_{2-x}O_3$, where $0.06 \le x \le 0.40$), the value of M(300 K/5 T) increases as the concentration of Al^{3+} ions increases.[66] The same behavior of M(300 K/5 T) is observed for Ga^{3+} substituting ions when the degree of doping does not exceed a threshold concentration limit (i.e., $x = 0.47$ for ε-$Ga_xFe_{2-x}O_3$), above which M(300 K/5 T) begins to decrease upon further Ga^{3+} substitution (i.e., when $0.47 \le x \le 0.67$).[65,85] In contrast, for

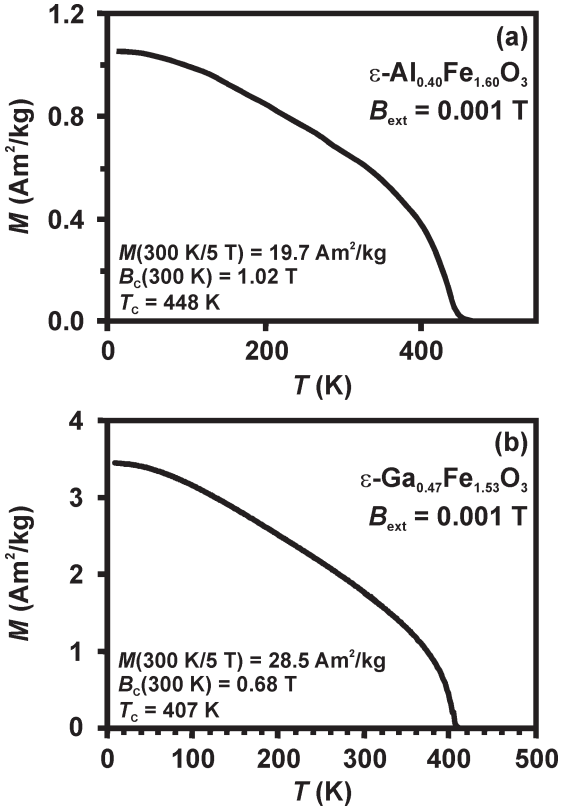

Figure 16. Temperature dependence of the magnetization (M) of representative Al^{3+}- and Ga^{3+}-doped ε-Fe_2O_3 nanosystems: (a) ε-$Al_{0.40}Fe_{1.60}O_3$ and (b) ε-$Ga_{0.47}Fe_{1.53}O_3$. (Panel (a) has been adapted from Namai et al.,[66] and panel (b) has been adapted from Ohkoshi et al.[65])

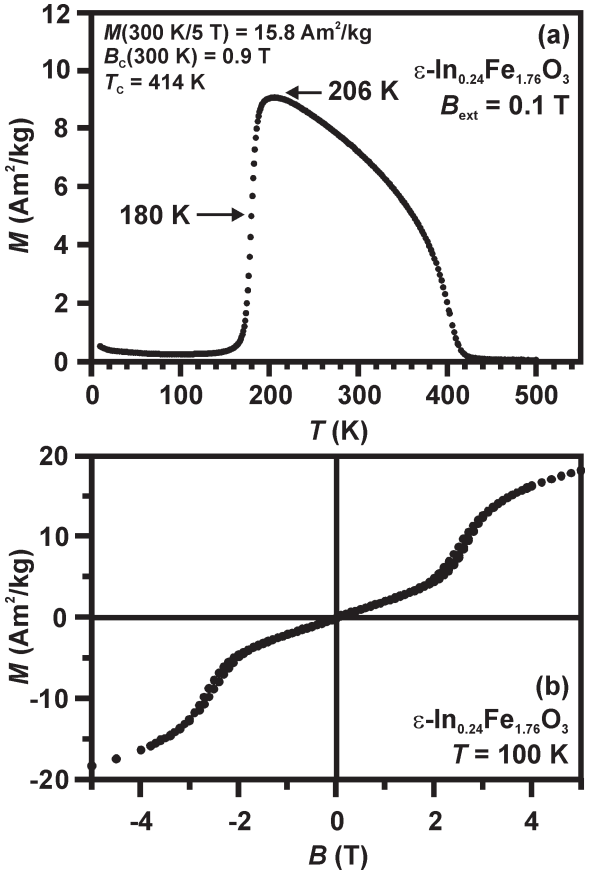

Figure 17. (a) Temperature dependence of magnetization (M) and (b) 100 K hysteresis loop of the representative In^{3+}-doped ε-Fe_2O_3 nanosystem. (Adapted from Sakurai et al.[86])

In^{3+}-substituted ε-Fe_2O_3 nanosystems (i.e., ε-$In_xFe_{2-x}O_3$, where $0.12 \leq x \leq 0.24$), M(300 K/5 T) values remain identical within the studied In^{3+} concentration range.[86] This can be explained based on the site substitution preference of doped ions. While In^{3+} ions preferentially occupy the distorted octahedral A- and B-sites, Al^{3+} and Ga^{3+} (below the threshold concentration limit) ions dominantly replace Fe^{3+} ions at the D-sites. Since the value of the net magnetization (or spontaneous magnetization) of ε-Fe_2O_3 is governed by the magnitude of the tetrahedral sublattice magnetization, the substitution of foreign ions taking place just at the D-sites enhances the overall magnetization of doped ε-Fe_2O_3. If the octahedral sites of the ε-Fe_2O_3 crystal structure are substituted, the net magnetization may remain unchanged or decrease, depending on the degree of substitution and location of doped ions.

The substitution of foreign ions also markedly influences the magnetic behavior of ε-Fe_2O_3 phase at low temperatures. For Ga^{3+}- and Al^{3+}-substituted ε-Fe_2O_3 nanoparticles and nanorods, no decrease in their magnetizations is observed below 110 K (see Figure 16), in contrast to the dramatic decrease in magnetization that has been reported for undoped ε-Fe_2O_3 (see Figure 14).[65,66,85] Instead, as evidenced from Figure 16, the magnetization of Ga^{3+}- and Al^{3+}-doped ε-Fe_2O_3 nanosystems continues to increase as the temperature decreases. In addition, Ga^{3+}- and Al^{3+}-substituted ε-Fe_2O_3 nanosystems do not suffer any magnetic softening below 150 K, but they do magnetically harden with decreasing temperature, as documented by their enhanced values of coercivity at 2 K, in comparison to those observed at 300 K.[65,66] Thus, Ga^{3+} and Al^{3+} substitution prevents a collapse in the coercivity and magnetic softening of the ε-Fe_2O_3 phase at low temperatures. Furthermore, it has been found that the difference between the values of the coercive field at 2 and 300 K gets bigger as the degree of substitution of Ga^{3+} and Al^{3+} ions increases.[65,66] This indicates that the degree of Ga^{3+} and Al^{3+} substitution controls the degree of magnetic hardening of Ga^{3+}- and Al^{3+}-doped ε-Fe_2O_3 nanosystems at low temperatures. In contrast, In^{3+}-substituted ε-Fe_2O_3 nanorods partially retain the low-temperature behavior of an undoped ε-Fe_2O_3 phase (i.e., a drastic decrease in the magnetization and coercivity collapse observed at low temperatures).[86] As the concentration of In^{3+} ions increases in the ε-Fe_2O_3 crystal structure, a decrease in the magnetization of In^{3+}-substituted ε-Fe_2O_3 nanorods, associated with a spin reorientation phenomenon, occurs at temperatures of >110 K (see Figure 17a). Moreover, the hysteresis loops of the ε-$In_{0.12}Fe_{1.88}O_3$ and ε-$In_{0.24}Fe_{1.76}O_3$ nanorod systems, measured at 100 K, exhibit unusual steps at $\sim$1.7 T and $\sim$2.5 T, respectively,[86] which is frequently observed for metamagnetic materials (see Figure 17b).[103] With regard to the in-field Mössbauer spectroscopy analysis performed by Tronc et al.,[24] Sakurai et al.[86] ascribed this behavior to a transition from an antiferromagnetic spin structure to a canted spin structure induced by an applied magnetic field. Supported also by the

heat capacity measurements, the temperature at which the spin reorientation phenomenon appears then has been interpreted as the temperature of the magnetic transition from a ferrimagnetic state to a low-temperature antiferromagnetic regime.[86] Thus, it seems that In^{3+} substituting ions probably change the low-temperature magnetic structure of the ε-Fe_2O_3 phase, which becomes similar to that characteristic of antiferromagnetic materials undergoing field-induced magnetic transitions. To confirm this effect of In^{3+} ions on the low-temperature magnetic arrangement of Fe^{3+} magnetic moments in the ε-Fe_2O_3 phase, measurements that enable monitoring of the local magnetic structure (e.g., neutron diffraction measurements) should be employed.

6. Magnetoelectric Properties of the ε-Fe_2O_3 Phase

Apart from remarkable magnetic properties, ε-Fe_2O_3 nanoobjects possess spontaneous polarization. This occurs because of the point group symmetry (*mm*2) exhibited by the ε-Fe_2O_3 room-temperature crystal structure, which belongs to a class of pyroelectric point groups. The existence of a polar axis in the crystal structure of the ε-Fe_2O_3 phase is responsible for the appearance of permanent electric dipole moments and, consequently, the generation of several physical phenomena, such as optical activity, piezoelectricity, and pyroelectricity. As the temperature decreases, there are substantial changes in the dielectric properties of ε-Fe_2O_3 observed at the temperatures around the magnetic transition.[17] In the temperature interval from 140 K down to 80 K, the permittivity value decreases by ~30%, which is connected with the changes in the electronic and phononic excitations. However, it was not absolutely clear if they act simultaneously or if one of them dominates over another one and thus preferentially drives modification in the permittivity of ε-Fe_2O_3 at ~110 K. A prediction that has been proposed by Gich et al.[17] and is based on the results of neutron powder diffraction, magnetization, and impedance measurements suggests that spin-dependent electronic excitations play a dominant role in the observed changes in permittivity. This indicates a tight connection between a magnetic state and dielectric permittivity. As the magnetic order changes at ~110 K, it is accompanied by a change in the dielectric constant of ε-Fe_2O_3. This magnetoelectric coupling has been formerly shown to exist in the orthorhombic phases of $HoMnO_3$ and $YMnO_3$ perovskites upon entering into an incommensurate magnetic arrangement.[104] In addition, it has been demonstrated that the dielectric permittivity of ε-Fe_2O_3 is sensitive to an applied magnetic field manifested by changes in its magnetocapacitance.[17] Such a magnetoelectric coupling in ε-Fe_2O_3 has been observed in no other single-metal ferrimagnetic oxide, thus making the ε-Fe_2O_3 phase very promising for magnetodielectric studies and possible applications such as electric/magnetic field-tunable devices and multiple-state-memory elements.[17]

7. Ferromagnetic Resonance and the ε-Fe_2O_3 Phase

Besides giant coercive field at room temperature and coupled magnetoelectric properties, the ε-Fe_2O_3 phase exhibits ferromagnetic resonance at ~190 GHz, because

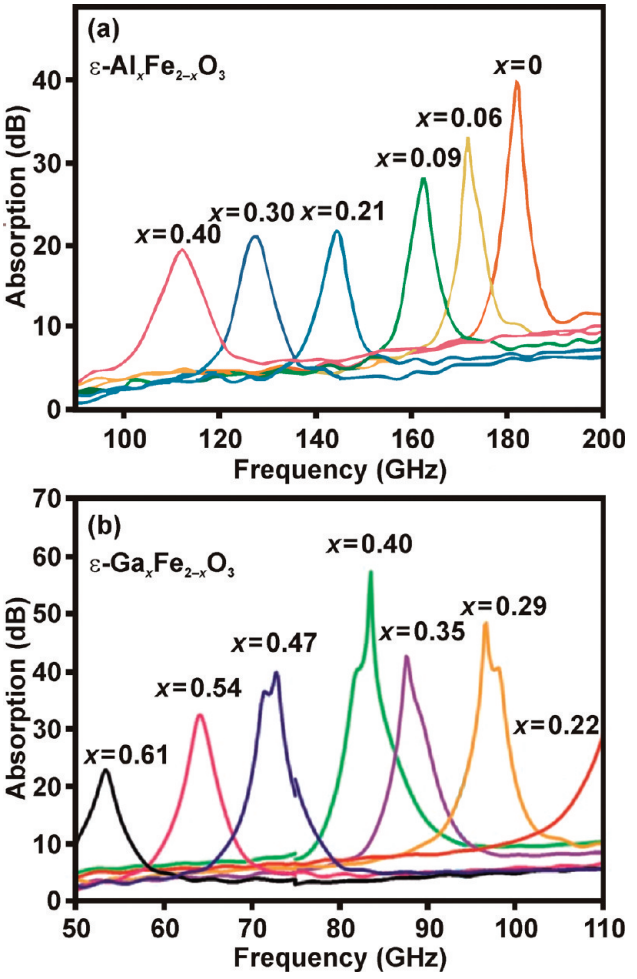

Figure 18. Millimeter-wave absorption spectra for (a) Al^{3+}-doped ε-Fe_2O_3 nanosystems and (b) Ga^{3+}-doped ε-Fe_2O_3 nanosystems showing the dependence of ferromagnetic resonance frequencies upon varying the degree of cation substitution. Panel (a) has been adapted from Namai et al.,[66] and panel (b) has been adapted from Ohkoshi et al.[65])

of a gyromagnetic effect.[65,66] The gyromagnetic effect is based on a precession of magnetization around the axis defined by the magnetocrystalline anisotropy field (H_{MC}). When an electromagnetic wave with a given frequency (f_{EM}) is applied to a ferromagnet, it is resonantly absorbed if $f_{EM} = f_r$, where f_r is the ferromagnetic resonance frequency. It is known that $f_r = (\eta/2\pi)H_{MC}$ where η denotes the gyromagnetic ratio.[54] If the sample contains randomly oriented magnetic particles, each with an uniaxial magnetic anisotropy, one can show that H_{MC} is proportional to the coercive field, so that $f_r \propto B_C$.[65,66] Thus, such a high f_r value of the ε-Fe_2O_3 phase is achieved by its large H_{MC} and B_C values. Since B_C can be easily tuned by a cation substitution, it is easy to get an absorber consisting of doped ε-Fe_2O_3 with a desired f_r value. For the ε-$Al_xFe_{2-x}O_3$ series with $0.06 \le x \le 0.40$ (see Figure 18a), the f_r values varied from ~172 GHz ($x = 0.06$) to ~112 GHz ($x = 0.40$), whereas, for the ε-$Ga_xFe_{2-x}O_3$ series with $0.10 \le x \le 0.67$ (see Figure 18b, showing only some representative samples with various Ga^{3+} concentrations), the f_r values fell within the range from ~147 GHz ($x = 0.10$) to ~35 GHz ($x = 0.67$). Figure 19 then demonstrates how f_r is dependent on B_C for ε-$Ga_xFe_{2-x}O_3$ nanorod systems with varying concentration of Ga^{3+} ions in the crystal structure of the ε-Fe_2O_3 phase.[65]

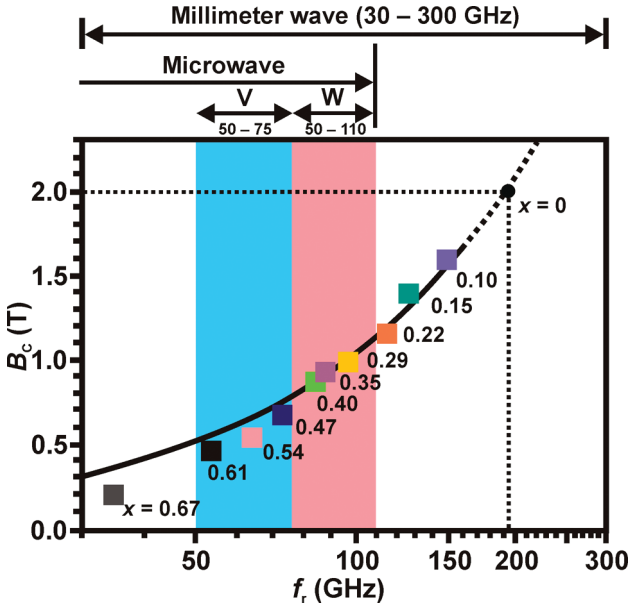

Figure 19. Relationship between the ferromagnetic resonance frequency (f_r) and the room-temperature coercivity (B_C) of ε-$Ga_xFe_{2-x}O_3$ nanosystems. (Adapted from Ohkoshi et al.[65])

By the time of their preparation and systematic study, ε-$Ga_xFe_{2-x}O_3$ nanosystems were determined to be the first magnetic materials exhibiting f_r values of >80 GHz.[65]

8. Conclusions and Future Perspective Studies of the ε-Fe_2O_3 Phase

We have presented a brief overview of the structural and magnetic properties of the ε-Fe_2O_3 phase, which, currently, is widely considered as a perspective candidate for applications based on high coercivity materials and/or requiring coupled electric and magnetic material characteristics and/or involving the absorption of electromagnetic waves with wavelengths on the order of units of millimeters (i.e., 30−300 GHz). We have shown how a combination of experimental techniques brings essential and valuable information on understanding the physicochemical properties of the ε-polymorph of Fe_2O_3, which remained unexplored for a long period of time and presently has attracted significant scientific attention, launched by the discovery of its giant coercivity at room temperature. Moreover, the interest in this magnetically appealing material has been greatly encouraged by an endeavor to synthesize it as a pure and stable phase, which has opened advanced synthetic approaches, leading to improved preparation procedures of the ε-Fe_2O_3 phase. At this time, low yields, a lack of precise control of the resulting product size, mixed phases, and the presence of impurities constitute reasons why it has not yet been fully exploited in the novel technologies. Nevertheless, recent preparation of the ε-Fe_2O_3 phase in the form of thin films may accelerate the endeavor to cope with these application-disincentive problems and initiates its future integration into various spintronic devices.

However, as felt throughout our review work, there is still a certain doubtfulness regarding the magnetic behavior of the ε-iron(III) oxide polymorph. The questionable areas, raised by several research works dealing with a description of magnetic responses of the ε-Fe_2O_3 phase at various temperatures and under an external magnetic field, especially concern the following issues: (i) the character of the room-temperature ground magnetic state of the ε-Fe_2O_3 phase (i.e., collinear ferrimagnet versus canted antiferromagnet); (ii) the magnetic transition at ~110 K (i.e., magnetic transition from a collinear ferrimagnetic structure to some incommensurate magnetic structure, most probably of a square-wave-modulated origin, versus the magnetic transition from one canted antiferromagnetic state (characterized by a certain value of the canting angle) to another canted antiferromagnetic state (with different canting angle), with the emergence of metamagnetic behavior at low temperatures); (iii) the possible occurrence of Morin-like magnetic transition below ~150 K, driven by a spin reorientation phenomenon taking place at particular magnetic sublattices of the ε-Fe_2O_3 phase; (iv) the definite explanation of an ε-Fe_2O_3 giant room-temperature coercive field and its collapse at low temperatures; and (v) the low-temperature magnetic structure of the ε-Fe_2O_3 phase changed and/or induced by cation substitution.

However, based on the experimental results from various measuring techniques, the authors, favoring different viewpoints concerning the room-temperature magnetic behavior of the ε-Fe_2O_3 phase and its evolution at low temperatures, seem to agree that the magnetic transition at ~110 K is governed by a series of structural transformations involving the tetrahedral sites and one type of octahedral (i.e., Fe_A) sites. In our opinion, this is the right starting point to understand the nature of the magnetic state of the ε-Fe_2O_3 phase. Thus, a combination of locally sensitive experimental techniques (i.e., nuclear magnetic resonance, in-field Mössbauer spectroscopy employed in parallel, perpendicular, or other geometry, neutron powder diffraction, etc.) may reveal information that would help to shed light upon the magnetism of this application-promising nanomaterial. Moreover, this experimental approach can clarify how a cation substitution, already known as a means to tuning the magnetic features of the ε-Fe_2O_3 phase, locally affects the magnetic structure of the ε-Fe_2O_3 phase.

In summary, there are two major challenges that must be addressed in future studies of the ε-Fe_2O_3 phase: (i) the search for optimal synthetic conditions to prepare single-phase ε-Fe_2O_3 with a high yield and the desired size and form, and thermally stabilize it; and (ii) the search for a correct description of the magnetic behavior of ε-Fe_2O_3 at temperatures below the characteristic magnetic ordering temperature. Solving these problems may thus significantly contribute to the introduction of this remarkable nanomaterial in various application fields and development of new convenient applications.

Acknowledgment. This work has been supported by the Operational Program Research and Development for Innovations − European Social Fund (Project No. CZ.1.05/2.1.00/03.0058 of the Ministry of Education, Youth and

Sports of the Czech Republic), the Ministry of Education, Youth and Sports of the Czech Republic (Project Nos. 1M6198959201 and MSM6198959218), and the Academy of Sciences of the Czech Republic (Project No. KAN115600801). The present research was supported in part by a Grant-in-Aid for Young Scientists (S) from JSPS, a Grant for the Global COE Program, "Chemistry Innovation through Cooperation of Science and Engineering", the Photon Frontier Network Program from MEXT of Japan, the Izumi Science and Technology Foundation, DOWA Technofund, the Asahi Glass Foundation, and the Shorai Foundation for Science and Technology. We are thankful for the Cryogenic Research Center, The University of Tokyo, Japan, and the Center for Nano Lithography & Analysis, The University of Tokyo, Japan, supported by MEXT Japan. A.N. is grateful for a JSPS Research Fellowship for Young Scientists.

References

(1) Teja, A. S.; Koh, A. S. *Prog. Cryst. Growth Charact. Mater.* **2009**, *55*, 22.
(2) Wu, W.; He, Q. G.; Jiang, C. Z. *Nanoscale Res. Lett.* **2008**, *3*, 397.
(3) Lu, A.-H.; Salabas, E. L.; Schuth, F. *Angew. Chem., Int. Ed.* **2007**, *46*, 1222.
(4) Cornell, R. M.; Schwertmann, U. *The Iron Oxides: Structure, Properties, Reactions, Occurrence and Uses*; Wiley−VCH: Weinheim, Germany, 2003.
(5) Gonzalez, J.; Chubykalo, O.; Gonzalez, J. M. In *Encyclopedia of Nanoscience and Nanotechnology*, Nalwa, H. S., Ed.; American Scientific Publishers: Stevenson Ranch, CA, 2004; Vol. *10*, p 1.
(6) Pankhurst, Q. A.; Connolly, J.; Jones, S. K.; Dobson, J. *J. Phys. D: Appl. Phys.* **2003**, *36*, R167.
(7) Tartaj, P.; Morales, M. D.; Veintemillas-Verdaguer, S.; Gonzalez-Carreno, T.; Serna, C. J. *J. Phys. D: Appl. Phys.* **2003**, *36*, R182.
(8) Berry, C. C.; Curtis, A. S. G. *J. Phys. D: Appl. Phys.* **2003**, *36*, R198.
(9) Mornet, S.; Vasseur, S.; Grasset, F.; Duguet, E. *J. Mater. Chem.* **2004**, *14*, 2161.
(10) Bulte, J. W. M.; Kraitchman, D. L. *NMR Biomed.* **2004**, *17*, 484.
(11) Gupta, A. K.; Gupta, M. *Biomaterials* **2005**, *26*, 3995.
(12) Laurent, S.; Forge, D.; Port, M.; Roch, A.; Robic, C.; Elst, L. V.; Muller, R. N. *Chem. Rev.* **2008**, *108*, 2064.
(13) Thorek, D. L. J.; Chen, A.; Czupryna, J.; Tsourkas, A. *Ann. Biomed. Eng.* **2006**, *34*, 23.
(14) Dormann, J. L.; Fiorani, D.; Tronc, E. In *Adv. Chem. Phys.*, Prigogine, I.; Rice, S. A., Eds.; John Wiley: New York, 1997; Vol. *98*, p 283.
(15) Zboril, R.; Mashlan, M.; Petridis, D. *Chem. Mater.* **2002**, *14*, 969.
(16) Jin, J.; Ohkoshi, S.; Hashimoto, K. *Adv. Mater.* **2004**, *16*, 48.
(17) Gich, M.; Frontera, C.; Roig, A.; Fontcuberta, J.; Molins, E.; Bellido, N.; Simon, C.; Fleta, C. *Nanotechnology* **2006**, *17*, 687.
(18) McClean, R. G.; Schofield, M. A.; Kean, W. F.; Sommer, C. V.; Robertson, D. P.; Toth, D.; Gajdarziska-Josifovska, M. *Eur. J. Mineral.* **2001**, *13*, 1235.
(19) Barcova, K.; Mashlan, M.; Zboril, R.; Martinec, P.; Kula, P. *Czech. J. Phys.* **2001**, *51*, 749.
(20) Petersen, N.; Schembera, N.; Schmidbauer, E.; Vali, H. *Phys. Chem. Miner.* **1987**, *14*, 118.
(21) Van Worterghem, J.; Mørup, S.; Villadsen, J.; Koch, C. J. H. *J. Mater. Sci.* **1987**, *22*, 438.
(22) Chanéac, C.; Tronc, E.; Jolivet, J. P. *Nanostruct. Mater.* **1995**, *6*, 715.
(23) Chanéac, C.; Tronc, E.; Jolivet, J. P. *J. Mater. Chem.* **1996**, *6*, 1905.
(24) Tronc, E.; Chanéac, C.; Jolivet, J. P. *J. Solid State Chem.* **1998**, *139*, 93.
(25) Jolivet, J. P.; Tronc, E.; Chanéac, C. *Eur. Phys. J.—Appl. Phys.* **2000**, *10*, 167.
(26) Zboril, R.; Mashlan, M.; Barcova, K.; Vujtek, M. *Hyperfine Interact.* **2002**, *139/140*, 597.
(27) Kelm, K.; Mader, W. *Z. Anorg. Allg. Chem.* **2005**, *631*, 2383.
(28) Kurmoo, M.; Rehspringer, J.-L.; Hutlova, A.; D'Orléans, C.; Vilminot, S.; Estournès, C.; Niznansky, D. *Chem. Mater.* **2005**, *17*, 1106.
(29) Gich, M.; Frontera, C.; Roig, A.; Taboada, E.; Molins, E.; Rechenberg, H. R.; Ardisson, J. D.; Macedo, W. A. A.; Ritter, C.; Hardy, V.; Sort, J.; Skumryev, V.; Noguès, J. *Chem. Mater.* **2006**, *18*, 3889.
(30) Schrader, R.; Buttner, G. *Z. Anorg. Allg. Chem.* **1963**, *320*, 320.
(31) Trautmann, J.-M.; Forestier, H. C. *C. R. Acad. Sci.* **1965**, *261*, 4423.
(32) Dérzi, I.; Coey, J. M. D. *Phys. Status Solidi A—Appl. Mater.* **1973**, *15*, 681.
(33) Tronc, E.; Chanéac, C.; Jolivet, J. P.; Grenèche, J.-M. *J. Appl. Phys.* **2005**, *98*, 053901.
(34) Ohkoshi, S.; Namai, A.; Sakurai, S. *J. Phys. Chem. C* **2009**, *113*, 11235.
(35) Rehspringer, J.-L.; Vilminot, S.; Niznansky, D.; Zaveta, K.; Estournès, C.; Kurmoo, M. *Hyperfine Interact.* **2005**, *166*, 475.
(36) Gich, M.; Roig, A.; Frontera, C.; Molins, E.; Sort, J.; Popovici, M.; Chouteau, G.; Martín y Marero, D.; Noguès, J. *J. Appl. Phys.* **2005**, *98*, 044307.
(37) Sakurai, S.; Jin, J.; Hashimoto, K.; Ohkoshi, S. *J. Phys. Soc. Jpn.* **2005**, *74*, 1946.
(38) Forestier, H.; Guiot-Guillain, G. C. *C. R. Acad. Sci.* **1934**, *199*, 720.
(39) Popovici, M.; Gich, M.; Niznansky, D.; Roig, A.; Savii, C.; Casas, Ll.; Molins, E.; Zaveta, K.; Enache, C.; Sort, J.; de Brion, S.; Chouteau, G.; Noguès, J. *Chem. Mater.* **2004**, *16*, 5542.
(40) Ohkoshi, S.; Sakurai, S.; Jin, J.; Hashimoto, K. *J. Appl. Phys.* **2005**, *97*, 10K312.
(41) Jin, J.; Hashimoto, K.; Ohkoshi, S. *J. Mater. Chem.* **2005**, *15*, 1067.
(42) Morber, J. R.; Ding, Y.; Haluska, M. S.; Li, Y.; Liu, J. P.; Wang, Z. L.; Snyder, R. L. *J. Phys. Chem. B* **2006**, *110*, 21672.
(43) Ding, Y.; Morber, J. R.; Snyder, R. L.; Wang, Z. L. *Adv. Funct. Mater.* **2007**, *17*, 1172.
(44) Kusano, Y.; Fujii, T.; Takada, J.; Fukuhara, M.; Doi, A.; Ikeda, Y.; Takano, M. *Chem. Mater.* **2008**, *20*, 151.
(45) Sakurai, S.; Tomita, K.; Hashimoto, K.; Yashiro, H.; Ohkoshi, S. *J. Phys. Chem. C* **2008**, *112*, 20212.
(46) Mori, K.; Oaki, Y.; Suda, M.; Einaga, Y.; Imai, H. *Chem. Lett.* **2008**, *37*, 814.
(47) Tadić, M.; Spasojević, V.; Kusigerski, V.; Marković, D.; Remškar, M. *Scr. Mater.* **2008**, *58*, 703.
(48) Brázda, P.; Nižňanský, D.; Rehspringer, J.-L.; Poltierová-Vejpravová, J. *J. Sol−Gel Sci. Technol.* **2009**, *51*, 78.
(49) Taboada, E.; Gich, M.; Roig, A. *ACS Nano* **2009**, *3*, 3377.
(50) Tseng, Y.-C.; Souza-Neto, N. M.; Haskel, D.; Gich, M.; Frontera, C.; Roig, A.; Van Veenendaal, M.; Noguès, J. *Phys. Rev. B* **2009**, *79*, 094404.
(51) Sakurai, S.; Shimoyama, J.-I.; Hashimoto, K.; Ohkoshi, S. *Chem. Phys. Lett.* **2008**, *458*, 333.
(52) Gich, M.; Roig, A.; Taboada, E.; Molins, E.; Bonafos, C.; Snoeck, E. *Faraday Discuss.* **2007**, *136*, 345.
(53) Gich, M.; Gazquez, J.; Roig, A.; Crespi, A.; Fontcuberta, J.; Idrobo, J. C.; Pennycook, S. J.; Varela, M.; Skumryev, V.; Varela, M. *Appl. Phys. Lett.* **2010**, *96*, 112508.
(54) Chikazumi, S. *Physics of Ferromagnetism*; Oxford University Press: Oxford, U.K., 1997.
(55) Sun, S.; Murray, C. B.; Weller, D.; Folks, L.; Moser, A. *Science* **2000**, *287*, 1989.
(56) Dronskowski, R. Adv. Funct. Mater. **2001**, *11*, 27 and references therein.
(57) Viswanathan, B.; Murthy, V. R. K. *Ferrite Materials: Science and Technology*; Springer−Verlag: Berlin, Germany, 1990.
(58) Batlle, X.; Labarta, A. *J. Phys. D: Appl. Phys.* **2002**, *35*, R15.
(59) Knobel, M.; Nunes, W. C.; Socolovsky, L. M.; De Biasi, E.; Vargas, J. M.; Denardin, J. C. *J. Nanosci. Nanotechnol.* **2008**, *8*, 2836.
(60) Weller, D.; Doerner, M. F. *Annu. Rev. Mater. Sci.* **2000**, *30*, 611.
(61) Piramanayagam, S. N. *J. Appl. Phys.* **2005**, *102*, 011301.
(62) Bader, S. D. *Rev. Mod. Phys.* **2006**, *78*, 1.
(63) Seemann, K.; Leiste, H.; Bekker, V. A. *J. Magn. Magn. Mater.* **2006**, *302*, 321.
(64) Ghasemi, A.; Hossienpour, A.; Morisako, A.; Saatchi, A.; Salehi, M. *J. Magn. Magn. Mater.* **2006**, *302*, 429.
(65) Ohkoshi, S.; Kuroki, S.; Sakurai, S.; Matsumoto, K.; Sato, K.; Sasaki, S. *Angew. Chem., Int. Ed.* **2007**, *46*, 8392.
(66) Namai, A.; Sakurai, S.; Nakajima, M.; Suemeto, T.; Matsumoto, K.; Goto, M.; Sasaki, S.; Ohkoshi, S. *J. Am. Chem. Soc.* **2009**, *131*, 1170.
(67) Taketomi, S.; Dai, Z. R.; Ohuchi, F. S. *J. Magn. Magn. Mater.* **2000**, *217*, 5.
(68) Taketomi, S.; Sorensen, C. M.; Klabunde, K. J. *J. Magn. Magn. Mater.* **2000**, *222*, 54.
(69) Sugasawa, M.; Kikukawa, N.; Nagano, Y.; Kayano, N.; Kimura, T. *Ceram. Int.* **2004**, *30*, 2191.
(70) Taketomi, S.; Shapiro, A. J.; Shull, R. D. *J. Appl. Phys.* **2003**, *93*, 7199.
(71) Battisha, I. K.; Afify, H. H.; Hamada, I. M. *J. Magn. Magn. Mater.* **2005**, *292*, 440.
(72) Kresge, C. T.; Leonowicz, M. E.; Roth, W. J.; Vartuli, J. C.; Beck, J. S. *Nature* **1992**, *359*, 710.
(73) Zhao, D.; Huo, Q.; Feng, J.; Chmelka, B. F.; Stucky, G. D. *J. Am. Chem. Soc.* **1998**, *120*, 6024.
(74) Doroshenko, V. N.; Kaurkovskaya, V. N.; Yakubenko, E. P.; Pobokin, D. I.; Entinzon, I. R.; Ogenko, V. M. *High Energy Chem.* **2002**, *36*, 157.
(75) Martelli, S.; Mancini, A.; Giorgi, R.; Alexandrescu, R.; Cojocaru, S.; Crunteanu, A.; Voicu, I.; Balu, M.; Morjan, I. *Appl. Surf. Sci.* **2000**, *154−155*, 353.
(76) Lančok, A.; Bezdička, P.; Klementová, M.; Závěta, K.; Savii, C. *Acta Phys. Pol., A* **2008**, *113*, 577.
(77) Viart, N. Elaboration by the sol-gel process of silica/iron oxides magnetic nanocomposites; Doctoral Thesis, Université de Strasbourg, Strasbourg, Alsace, France, 1996.
(78) Hutlova, A. Preparation of magnetic nanocomposites using sol-gel method and their characterization; Doctoral Thesis, Université de Strasbourg, Strasbourg, Alsace, France, 2003.
(79) Walter-Levy, L.; Quemeneur, M. E. *C. R. Acad. Sci.* **1963**, *257*, 3410.

(80) Nižňanský, D.; Rehspringer, J.-L.; Drillon, M. *IEEE Trans. Magn.* **1994**, *30*, 821.
(81) Tucek, J.; Zboril, R.; Petridis, D. *J. Nanosci. Nanotechnol.* **2006**, *6*, 926.
(82) Barick, K. C.; Varaprasad, B. S. D.; Ch., S.; Bahadur, D. *J. Non-Cryst. Solids* **2010**, *356*, 153.
(83) Dormann, J. L.; Viart, N.; Rehspringer, J. L.; Ezzir, A.; Niznansky, D. *Hyperfine Interact.* **1998**, *112*, 89.
(84) Sakurai, S.; Namai, A.; Hashimoto, K.; Ohkoshi, S. *J. Am. Chem. Soc.* **2009**, *131*, 18299.
(85) Namai, A.; Sakurai, S.; Ohkoshi, S. *J. Appl. Phys.* **2009**, *105*, 07B516.
(86) Sakurai, S.; Kuroki, S.; Tokoro, H.; Hashimoto, K.; Ohkoshi, S. *Adv. Funct. Mater.* **2007**, *17*, 2278.
(87) Greenwood, N. N.; Gibb, T. C. *Mössbauer Spectroscopy*; Chapman and Hall, Ltd.: London, 1971.
(88) Chappert, J. *J. Phys. Colloque* **1974**, *35*, C6–71.
(89) Thomas, M. F.; Johnson, C. E. In *Mössbauer Spectroscopy*; Dickson, D. P. E.; Berry, F. J., Eds.; Cambridge University Press: Cambridge, U.K., 1986; p 143.
(90) Morin, F. *Phys. Rev.* **1950**, *78*, 819.
(91) Morrish, A. H. *Canted Antiferromagnetism: Hematite*; World Scientific Publishing Company: Singapore, 1994.
(92) Dzyaloshinsky, I. *J. Phys. Chem. Solids* **1958**, *4*, 241.
(93) Moriya, T. *Phys. Rev.* **1960**, *120*, 91.
(94) Vandenberghe, R. E.; de Grave, E.; Landuydt, C.; Bowen, L. H. *Hyperfine Interact.* **1990**, *53*, 175.
(95) Tronc, E.; Prene, P.; Jolivet, J. P.; Dormann, J. L.; Grenèche, J.-M. *Hyperfine Interact.* **1998**, *112*, 97.
(96) Serna, C. J.; Bødker, F.; Mørup, S.; Morales, M. P.; Sandiumenge, F.; Veintemillas-Verdaguer, S. *Solid State Commun.* **2001**, *118*, 437.
(97) Morrish, A. H.; Haneda, K. *J. Appl. Phys.* **1981**, *52*, 2496.
(98) Kodama, R. H.; Berkowitz, A. E.; McNiff, E. J., Jr.; Foner, S. *Phys. Rev. Lett.* **1996**, *77*, 394.
(99) Johnson, C. E. *J. Phys. D—Appl. Phys.* **1996**, *29*, 2266.
(100) Casas, Ll.; Roig, A.; Molins, E.; Grenèche, J.-M.; Asenjo, J.; Tejada, J. *Appl. Phys. A—Mater. Sci. Process* **2002**, *74*, 591.
(101) Li, H.-S.; Coey, J. M. D. In *Handbook of Magnetic Materials*; Buschow, K. H. J., Ed.; North−Holland: Amsterdam, 1992; Vol. *6*, p 1.
(102) Hutlova, A.; Niznansky, D.; Rehspringer, J.-L.; Estournès, C.; Kurmoo, M. *Adv. Mater.* **2003**, *15*, 1622.
(103) Stryjewski, E.; Giordano, N. *Adv. Phys.* **1977**, *26*, 487.
(104) Lorenz, B.; Wang, Y. Q.; Sun, Y. Y.; Chu, C. W. *Phys. Rev. B* **2004**, *70*, 212412.